International Journal of Greenhouse Gas Control 94 (2020) 102924

Contents lists available at ScienceDirect

International Journal of Greenhouse Gas Control

journal homepage: www.elsevier.com/locate/ijggc

Swelling clay minerals and containment risk assessment for the storage seal of the Peterhead CCS project

A. Busch[a,*], S.J.T. Hangx[b], J.D. Marshall[c], H.M. Wentinck[c]

[a] Heriot-Watt University, Lyell Centre, Research Avenue S, EH14 4AS Edinburgh, Scotland, UK
[b] High Pressure and Temperature Laboratory, Department of Earth Sciences, Faculty of Geosciences, Utrecht University, P.O. Box 80.021, 3508 TA Utrecht, the Netherlands
[c] Shell Global Solutions B.V., Kesslerpark 1, 2288 GS Rijswijk, the Netherlands

ARTICLE INFO

Keywords:
Peterhead CCS project
Clay swelling
Caprock
Risk assessment
Containment

ABSTRACT

Coupled modelling, based on laboratory data, indicated that the storage seal above the Captain reservoir of the Peterhead CCS project could be affected by stresses caused by clay swelling due to CO_2 interaction. In particular, calculations indicate that, over a period of 100 – 10,000 years, local shear failure in rock exposed to CO_2 may occur under unfavourable stress conditions. The likelihood and consequences of local shear failure are however difficult to assess. We therefore defined passive safeguards against this potential risk to seal integrity. The basis for these safeguards is data and information given in the Peterhead CCS Storage Permit Application (storage seal thicknesses, lithologies, reservoir conditions etc.), chemical, thermodynamic and mechanical data from laboratory measurements, as well as the coupled model built and described earlier by Wentinck and Busch (2017).

The passive safeguards provided in this study address the mineralogy of the caprock and more specifically its swellable clay content. Furthermore, the geometry of the reservoir is addressed, particularly with respect to the presence of pre-existing faults. Our model shows that for shear failure to be a risk a fault offset on the order of the thickness of the sealing layer needs to be present and in contact with the CO_2 plume. It should be noted that swelling stress build-up may relax by creep of the surrounding shale matrix, thereby buffering this effect. Finally, the risk of CO_2 to escape the storage container only exists when slip on pre-existing faults leads to permeability enhancement as well as reduction of capillary entry pressures along the fault.

Our analyses show that the smectite contents of the unit at the base of the caprock is significant with an average of 57 %, substantiating the threat of clay swelling. Taking the locations of interpreted faults and the total storage seal thickness of 117 – 165 m, we find no potential offsets similar to this thickness, as identified offsets are up to 33 m. Unquantified uncertainties remain in the creep behaviour of the caprock as well as the fault permeability. Given however that a maximum fault offset is lower than the seal thickness, we classify loss of containment due to fault reactivation caused by swelling clays, and concomitant fluid leakage, to be a low geological risk for the Peterhead CCS project.

1. Introduction

Until 2015 Shell U.K. Limited had proposed to store 20 million tonnes of high purity CO_2 in a subsurface volume centred at the depleted Goldeneye gas condensate field, Outer Moray Firth, UK continental shelf as part of a UK Government CCS Commercialisation Competition. The proposed source of CO_2 was the Peterhead Power Station in Aberdeenshire, providing approximately 10 million tonnes of > 99 % purity CO_2 over a period of 10–15 years. The CO_2 was planned to be transported from the Peterhead Power Station directly offshore via pipeline to the Goldeneye platform above the field, located ~100 km northeast of Peterhead, Aberdeenshire in water of ~120 m depth. It was aimed to inject the CO_2 into the depleted Goldeneye field reusing the existing hydrocarbon production wells, at a maximum rate of just over 1 million tonnes p.a. The Goldeneye field is situated in the Outer Moray Firth on the northern margin of the South Halibut Basin and has a combined structural and stratigraphic trap of Lower Cretaceous Captain Sandstone Member (Shell UK Ltd., 2014a). Shell U.K. Limited had finalised the Front-End Engineering and Design (FEED) study for this project, which has been disseminated via the

* Corresponding author at: Heriot-Watt University, Lyell Centre, Research Avenue S, EH14 4AS Edinburgh, Scotland, UK.
E-mail address: a.busch@hw.ac.uk (A. Busch).

https://doi.org/10.1016/j.ijggc.2019.102924
Received 19 March 2019; Received in revised form 11 November 2019; Accepted 24 November 2019
Available online 10 December 2019
1750-5836/

websites of the UK government.[1] The project was halted when the UK Department of Energy and Climate Change (now part of UK Department for Business, Energy & Industrial Strategy) announced funding cuts for the CCS Commercialisation Competition in November 2015.

In this study we assess the potential for clay swelling induced stress build-up that may lead to fault reactivation and the associated creation of a leak path. A model was developed for the transport of CO_2-rich brine through a shale-type caprock. This model is based on and calibrated for literature data, using the combined poroelastic response of fluid transport, following sorption of aqueous CO_2 and swelling in the pore space of tight rocks such as shales (Wentinck and Busch, 2017). The basic concept known from wellbore stability studies is that swelling clays, like smectite, can volumetrically swell or shrink when reservoir conditions change (van Oort, 2003).

Previously, we have shown in laboratory tests that, under certain conditions, swelling clays develop a swelling strain and swelling stress when in contact with CO_2. The volumetric swelling of the interlayer space of unconfined pure smectite can be more than 10 % pending on the hydration state of the clay (de Jong et al., 2014; Giesting et al., 2012a, b; Rother et al., 2013; Schaef et al., 2012; Zhang et al., 2018). The swelling stress can be more than 30 MPa under isovolumetric conditions and under effective stress conditions representative for reservoir depths of 1500 − 2500 m (for a full review, see Busch et al., 2016; Zhang et al., 2018). As long as CO_2 is not displacing water in the caprock, the time scales for migration of CO_2 in low permeability rocks are diffusion-driven. With diffusion coefficients being on the order of 10^{-10}–10^{-12} $m^2 s^{-1}$ (Busch et al., 2008; Busch and Kampman, 2018), this relates to CO_2 migration rates on the order of millimeters per year.

Smectite is a swellable clay, indicative of shallow, immature fine-grained sedimentary rocks, which transforms into non-swellable illite with increasing burial depth (pressure, temperature) (Altaner and Ylagan, 1997). Sediments in the North Sea are relatively immature and it is frequently reported that they contain moderate to high amounts of smectite (Pearson and Small, 1988), mainly as illite/smectite (I/S) mixed-layers.

Pearson (1990) evaluated I/S contents of regional shale formations in the North Sea and total smectite contents, as shown in Fig. 1. Clay composition of total mineralogy is not given in the study by Pearson but assumed to be > 50 % due to the clay-rich nature of shales or mudrocks. Since the I/S values are averaged over different wells, they cannot be plotted versus total depth. Nevertheless a general decrease in I/S and total smectite contents is shown with geological age and therefore burial depth.

The Captain Sandstone of the Goldeneye reservoir is sealed by a combination of the Cretaceous Upper Valhall and Rødby mudrocks of the Cromer Knoll Group and the overlying Hidra and Plenus Marl Formations of the Chalk Group. The Upper Valhall and Rødby mudrocks are defined as the caprock, being in direct contact with the Captain Sandstone, the Upper Valhall in the south and west, the Rødby in the north east. The Hidra and Plenus Marls are interbedded carbonates and mudstones, considered to act as an additional low permeability barrier to upwards migrating fluids. As part of the geological assessment of the Peterhead CCS project, preliminary mineralogical analysis suggested that the Upper Valhall and Rødby mudrocks contain combined smectite and I/S contents of up to 50–60 %, in line with the trends observed by Pearson (1990, see Fig. 1).

The aim of this study is to assess whether changes in rock properties due to CO_2-water-rock interactions determined in the laboratory or indicated from modelling studies can potentially cause a risk to CO_2 storage in general or CO_2 leakage in particular. However, such observations need to be put in context of the specific conditions of the CO_2 store by understanding natural or geological barriers (passive safeguards) that would prevent unexpected changes of the petrophysical, geochemical or mechanical properties of the reservoir or seal formation. Passive safeguards are geological, reservoir-specific features that can prevent a specific risk. Site-specific assessment is therefore important in order to create a realistic rather than a hypothetical case.

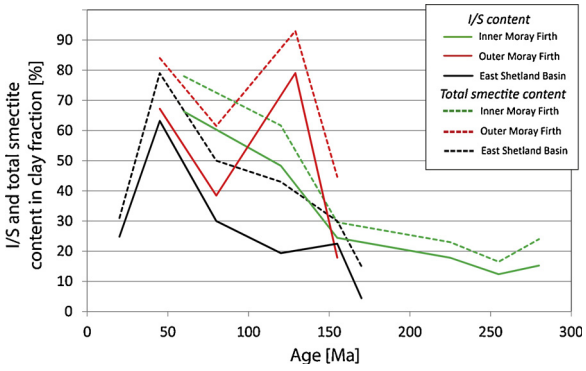

Fig. 1. Illite/smectite (I/S) contents of total clay content (< 2 µm fraction; solid lines) and total smectite contents of I/S (dashed lines) for different parts of the North Sea in the vicinity of the Peterhead CCS project location. Note that age can be considered a rough measure for burial depth, i.e. increasing age means increasing burial depth (data from Pearson (1990)).

For the Peterhead CCS project, we identified four risk factors that in combination may impact seal integrity, leading to loss of containment: (i) high amounts of smectite in the caprock, (ii) pre-existing faults with significant offsets, (iii) significant swelling stresses that do not relax into the shale matrix and (iv) the creation of a permeable pathway along a pre-existing fault. In the following, we discuss the passive safeguards (mineralogy, geometry, mechanical behaviour and transport properties) in the framework of the Peterhead storage complex in order to determine the likelihood of leakage of CO_2 from the storage site along faults experiencing slip induced by CO_2-clay interactions driving stress changes in the caprock directly overlying the storage reservoir. We will do so using field and laboratory data, combined with modelling predictions. Given the laboratory-based evidence for CO_2-induced clay swelling, our modelling results can be transferred to the Goldeneye storage complex of the Peterhead CCS project (for details see Wentinck and Busch, 2017).

2. Geology of the goldeneye storage complex

Following the Peterhead CCS Storage Permit Application (Shell UK Ltd., 2014a) and the EU directive (Commission of the European Communities, 2009) the following definitions apply and are put in context to the Goldeneye CO_2 store. The *storage complex* is composed of the storage site and the surrounding geological domain, which can have an effect on overall storage integrity and security. The surrounding geological domain is defined to contain the *storage seal*, the *secondary container*, and the *complex seal*. A stratigraphic overview including thicknesses (where possible) is given in Fig. 2. Accordingly, the storage seal thickness varies between 117 and 165 m in total and consists of mudrocks (Upper Valhall and Rødby Fm, > 30 m, av. 60 m) and two formations characterised by tight chalk with interbedded mudstone (Hidra and Plenus Fms.).

2.1. Storage site

The *storage site* is defined as the volume within a geological formation used for the storage of CO_2 and associated surface and injection facilities. In this study the storage site, or primary container, for the CO_2 that was planned to be stored from the Peterhead Power Station, is the volume centered on the depleted Goldeneye gas condensate field. The site is defined as the pore volume between the mapped top of the

[1] https://www.gov.uk/government/publications/carbon-capture-and-storage-knowledge-sharing-technical-subsurface-and-well-engineering.

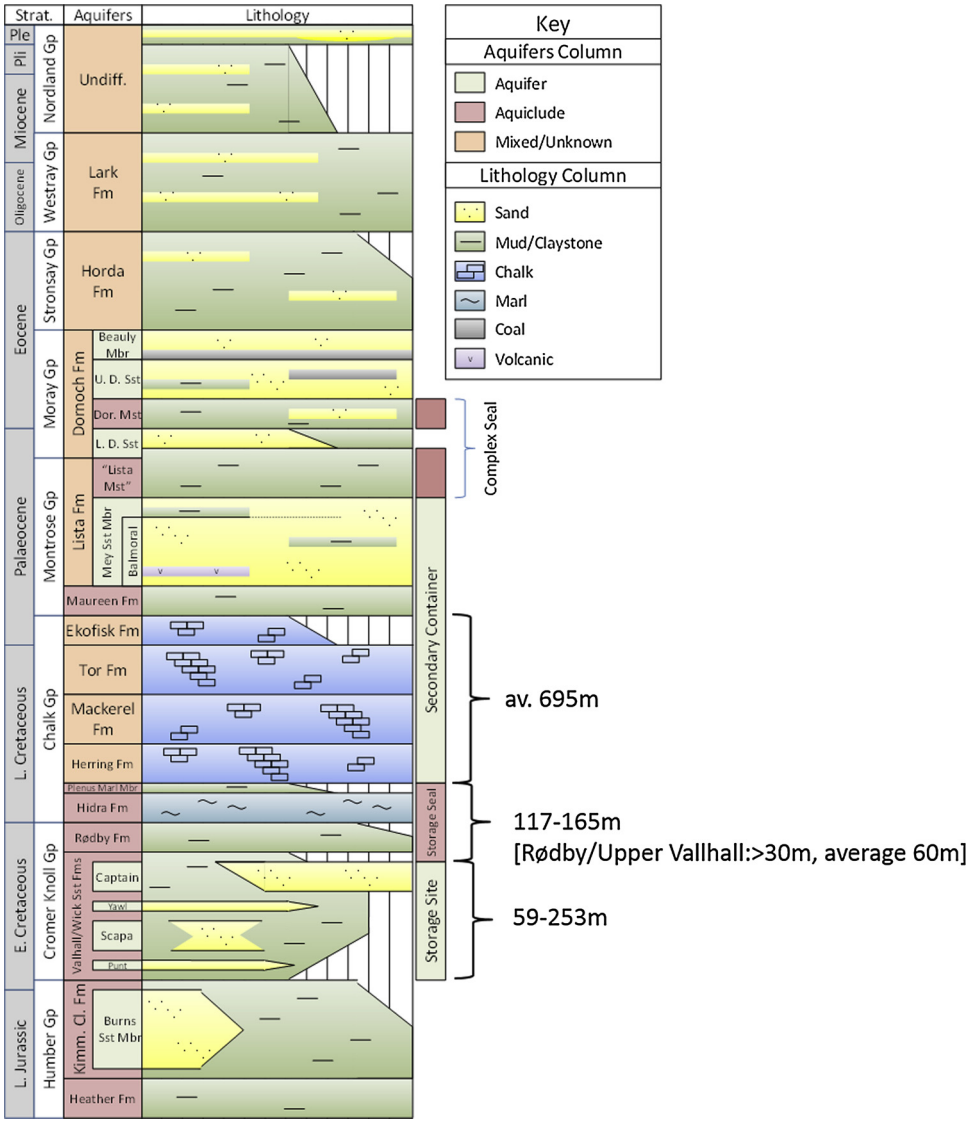

Fig. 2. Storage complex consisting of storage site, storage seal, secondary container and complex seal. Thicknesses have been added where data was available. Stratigraphic column modified from Peterhead CCS Storage Permit Application (Shell UK Ltd., 2014a).

Kimmeridge Clay Formation and the mapped top of the Captain Sandstone Member of the Upper Valhall Formation. It exists within an area bounded by a polygon that lies a short distance beyond the original oil-water-contact (OOWC) of the Goldeneye field. Porous and permeable lithologies exist within the Scapa Sandstone, Yawl Sandstone and Captain Sandstone Members of the Valhall Formation. The Captain Sandstone is the produced hydrocarbon reservoir of the Goldeneye field. More details on exact locations can be obtained from the Peterhead CCS Storage Permit Application (Shell UK Ltd., 2014a).

2.2. Storage seal

The *storage seal* includes the Upper Valhall Member of the Valhall Formation and the Rødby Formation – both part of the Cromer Knoll Group and together considered the caprock for the field – and the Hidra Formation and Plenus Marl Bed, which represent the lower Chalk Group. The lower parts of the storage seal consist of mudrocks with sporadic thin beds of argillaceous limestone. The Upper Valhall shale directly overlies the Captain Sandstone in the southern three quarters of the field. In the northern quarter, the Upper Valhall thins out and the Rødby shale oversteps the Valhall unit directly overlying the Captain Sandstone. Over the extent of the storage site, the Rødby alone is at least 30 m thick with an average thickness of 60 m.

In the lower Chalk Group intervals the Hidra Formation consists of bioturbated limestones with interbedded mudstones, while the Plenus Marl Bed is a relatively thin unit of black mudstone, both forming sealing layers. They act as a seal over parts of the Captain Field in the Inner Moray Firth (Pinnock et al., 2003). They are also a seal to hydrocarbons in the Central North Sea where compacted low porosity/permeability chalk sits unconformably on the high-pressure Skua and Judy clastic reservoirs of Jurassic age and the Marnock reservoir of Triassic age (Casabianca and Cosgrove, 2012).

The thickness of the storage seal as a whole varies from 117 m in the north to 165 m in the south

2.3. Hydraulically connected secondary container in the (lateral) underburden

The hydraulically connected secondary storage container can accommodate migration of CO_2 within the reservoir formations but also laterally beyond the licensed boundary of the *storage site*. The Captain Sandstone Member itself is interpreted to be present along a 180 km east-west system termed the Captain Fairway. The underlying Yawl and Scapa Sandstone Members of the Kimmeridge Clay Formation are also

part of the storage site and offer potential secondary storage. Data from wells to the west of the Goldeneye field shows that both sandstones are absent in this direction, though an older sandstone unit – the Punt Sandstone Member, is penetrated. To the east of the *storage site*, well data shows that the Scapa Sandstone Member thins out in this direction. The Yawl Sandstone is seen in wells over several tens of kilometers east of Goldeneye.

2.4. Secondary container in the overburden

The *secondary storage* (*overburden*) for the Goldeneye field includes the upper Chalk Group (above the top of the Plenus Marl Bed), the Montrose Group (particularly the Mey Sandstone Member) and the lower Dornoch sandstone within the Moray Group. Overall, the ~700 m thick Chalk Group will act as an effective secondary seal to the injected CO_2 in the Captain Sandstone of the Goldeneye Field, with petrophysical and analogue evidence indicating that the deeper formations, the Herring, Plenus Marl and Hidra are present across the entire Goldeneye Field and contain sufficient clay to represent a seal to vertical fluid movements. Cemented intervals are also present and would provide significant baffling of vertical fluid flow.

The Montrose Group (Palaeocene) contains the Lista Formation which is characterised by the presence of interbedded sandstones and mudstones. At the top of the Lista Formation is an un-named mudstone-dominated facies which is one of two regionally continuous mudstones that are identified as the *complex seal* (see Section 2.5).

2.5. Complex seal

The Lista mudstone and Dornoch mudstone were identified as the *complex seal* because they can be reliably correlated in all wells within the *storage complex*. Furthermore, they are found at depths greater than 800 m true vertical depth subsea across the entire area under investigation and the nearest outcrop of these units is interpreted to be > 150 km away from the *storage site*. Two of the abandoned exploration wells have plugs set at either Lista or Dornoch mudstone level.

3. Poro-elastic effects of clay swelling by CO_2 and implications for shear failure of the caprock

3.1. Mechanical description of the shaly caprock

In relatively immature or shallow mudrock layers such as the Rødby mudrock, flaky clay platelets of smectites are more or less aligned and compacted to form aggregates or conglomerates. The platelets can be distorted or wrinkled. Relatively weak chemical bonds, electrostatic and/or capillary forces between the clay platelets give stiffness and cohesive strength to the rock. Other minerals, like quartz, calcite and organic material can be mixed with the clay conglomerates. They can also bond to the clay platelets forming a 'cement' contributing to mechanical rock strength.

Within the mudrock we distinct two types of pore volumes. The first pore volume consists of connected micro-, meso- and macropores and micro-cracks. From here on we refer to them as macropores. The second pore volume consists of the interlayer space between the clay layers of the smectite platelets in this rock, as shown in Fig. 3. Depending on the hydration state of the clay, the interlayer space can expand considerably when the CO_2 concentration in this pore volume increases.

The repulsive pressure in the interlayer space between the clay layers balances with the other mechanical forces on the clay platelets. These forces are the field stresses caused by the burial load and the cohesive forces in the composite. Part of the micro-strain generated by swelling or shrinkage of the interlayer space in the clay platelets relaxes into the macropore volume.

The Rødby mudrock is organic lean. So, we disregard CO_2 sorption in organic matter. Furthermore, we assume that there are no leaking natural fractures of major macroscopic dimensions in the caprock. Such fractures would have resulted in an escape of the natural gas from the reservoir to the surface but no evidence has been found for this.

3.2. General model

To predict shear failure in the caprock due to clay swelling, we use a two dimensional extension of the model developed by Wentinck and Busch (2017). This macroscopic model describes the elastic deformation of shale due to diffusion and to pressure driven flow of CO_2 dissolved in brine. For details about the equations used, including those for the pressures in the macropores and in the interlayer space, and a complete list of the input parameters of the model, we refer to the original reference.

The main features and assumptions of the model are as follows: The reservoir-caprock interface is modelled as a sharp and smooth interface. The caprock is modelled as a macroscopic isotropic and uniform linear poro-elastic rock on top of a poro-elastic reservoir. Conservatively, we disregard the plastic/ductile properties of the clay-rich caprock, although they can be important at long time scales to relax the stress in the caprock following from slow deformations. We further disregard macroscopic mechanical anisotropy in terms of rock strength and the build-up of swelling stresses which may follow from the alignment of the clay platelets and micro-fractures along bedding planes of the caprock. Clay minerals are typically oriented perpendicular to the largest principle stress which is usually the overburden stress. Swelling stress would therefore mainly develop into the vertical direction which has already been shown experimentally by de Jong et al. (2014) and Zhang et al. (2018). The differences appear to be much less than an order of magnitude and can be disregarded at this stage of the study.

The fluid pressure in the reservoir and in the macropores of the caprock are assumed to be the same and hydrostatic when the CO_2 plume reaches this interface and are supposed to remain constant over time. We disregard some pressure decrease by pressure diffusion in the caprock near the interface during the years of gas production. The constant reservoir pressure is in line with modest pressure changes predicted by reservoir modelling after the injection of CO_2, keeping in mind that the long term prediction depends on less constrained inflow of water from nearby aquifers and on pressure effects from other depleted gas fields in the region. So, without imposing a change in the fluid pressure at the reservoir-caprock interface, we highlight in this study primarily the effect of diffusional transport of CO_2 in the caprock. Furthermore, we expect that the increase of the hydrostatic pressure at the reservoir-caprock interface by the formation of a CO_2 column in the reservoir is moderate, i.e. about 0.35 MPa, corresponding to a CO_2 gas column height on the order of 100 m, see Section 4.4.

We disregard small changes and gradients in the temperature of the caprock over time and assume that the temperature of the CO_2 is approximately the same as the temperature before gas production at the reservoir-caprock interface.

As defined above, the porous caprock has two distinct types of pore volumes, i.e. the macropores and the interlayer space. We assume that CO_2 and water transport through the caprock occurs only through the connected macropore volume of the caprock. In the model, the transport of these species through the macropore volume is solved by general and standard macroscopic reactive diffusive-convective transport equations for CO_2 and water and the equation of macroscopic fluid motion in porous rocks which can be found in classical textbooks on fluid flow, see for example Bird et al. (2007). The transport equations include effects of fluid compressibility and Darcy's law for convective flow due to macroscopic pressure gradients over the macropore volume and include diffusional flow driven by concentration gradients of both species. The brine in the caprock is of low-to-moderate salinity and modelled as a single species, i.e. water.

In our simulations, the diffusive transport appears to be dominant as

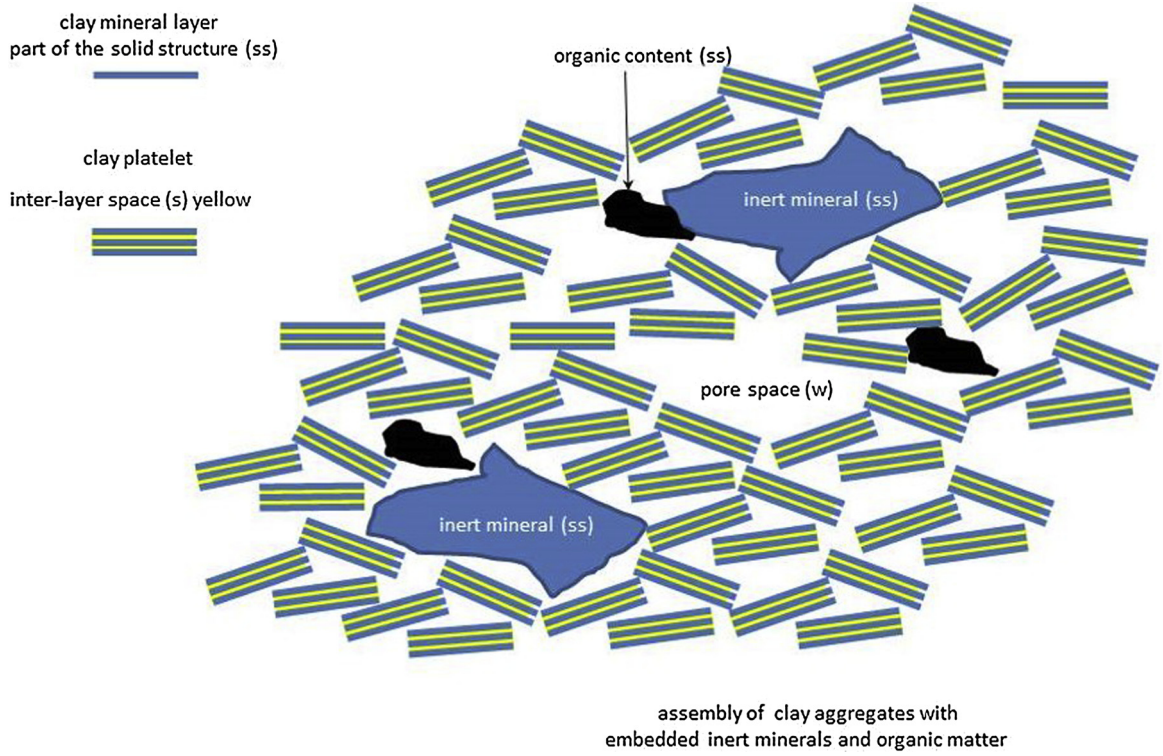

Fig. 3. Concept of a poro-elastic caprock or mudrock with clay and with two distinct different pore volumes. The water and CO_2 molecules in the interlayer space between the clay layers are differently organised or in another phase than in the connected macropore volume between the clay platelets. In good approximation, the molecules behave in the pore volume as in a bulk fluid. Fluid motion in the macropores is possible by diffusion and pressure gradients.

there is no imposed pressure change at the reservoir-caprock interface foreseen. Pressure gradients in the macropores of the caprock following from the deformation of this rock are small and the related fluid transport is insignificant. The diffusion coefficient used is a macroscopic effective diffusion coefficient accounting for diffusion in a microscopically heterogeneous porous rock. We use conservative values for the permeability and the diffusion coefficient when compared to typical values measured for comparable mudrocks. The effective diffusion coefficient depends on the same connectivity between the macropores as the permeability of the caprock. Hence, we assume that this constant reduces in a similar manner as the permeability when the effective stress in the caprock increases, see below. Conservatively, we disregard possible mineral reactions involving dissolved CO_2 which could slow down the migration of CO_2 in the caprock (Kampman et al., 2016).

In two simulations, we include a possible significant increase in the permeability and diffusion coefficient when the caprock approaches a condition of shear failure. It has been reported that the permeability of faults or sheared rock in Opalinus clay can increase between one to two orders of magnitude from lab experiments and field observations (Laurich et al., 2014; Makhnenko et al., 2017).

CO_2 and water in the macropores and in the interlayer space of the clay platelets are considered to be in local thermodynamic equilibrium where 'local' is small compared to macroscopic dimensions. This is a fair assumption as the transport of CO_2 and water through the connected macropores by convective flow and diffusion over macroscopic distances can generally be considered slower than the local exchange rate of these species between the macropores and the interlayer space connected to these macropores. This exchange is by local diffusion on a microscopic scale. Local thermodynamic equilibrium in a macroscopic sense follows directly from the minimisation of the total free energy density of the system. This means that the chemical potentials of CO_2 in both pore volumes are locally equal (and the same holds for water) and it means that there is local mechanical equilibrium in the poro-elastic rock. The task is therefore to define suitable expressions for changes in the chemical potentials of both species and a suitable expression for changes in the free elastic energy of the poro-elastic rock.

Expressions for changes in the chemical potentials of both species in both pore volumes follow from ideal and non-ideal mixing theory underlying osmotic-like processes. The expressions include appropriate work terms defined by changes in fluid pressures and in the partial molar volumes of the species in both pore volumes. Equal chemical potentials imply that the fluid pressures in the macropores and in the interlayer space can be quite different and this osmotic effect leads to volume changes or swelling of the interlayer space.

The different fluid pressures in both pore volumes and the volume changes of both pore volumes must be consistent with poro-elastic deformations. To account for that, the expression for a change in the free elastic energy density of the poro-elastic medium, as defined by Biot (1962), must be expanded by more terms, as explained in Wentinck and Busch (2017). As such, the expression becomes a function of three independent variables instead of two. These are the changes in the strain tensor in the rock (which is seen as one variable although it has several independent components) and the changes of the fluid contents in two types of pore volumes instead of one pore volume. Taking the appropriate derivates of the change in the free elastic energy to these variables, we obtain expressions for the stresses in the rock and for the fluid pressures in both pore volumes.

The model has been implemented in COMSOL™. The numerical solver solves implicitly and fully coupled all partial differential equations involving fluid transport, chemical equilibrium and rock deformation with a fine boundary layer mesh near the reservoir-caprock interface. Expressions for changes in the chemical potentials in terms of changes in pressures and concentrations follow from integrating incremental changes during the simulation while the coefficients in these expressions vary with the conditions.

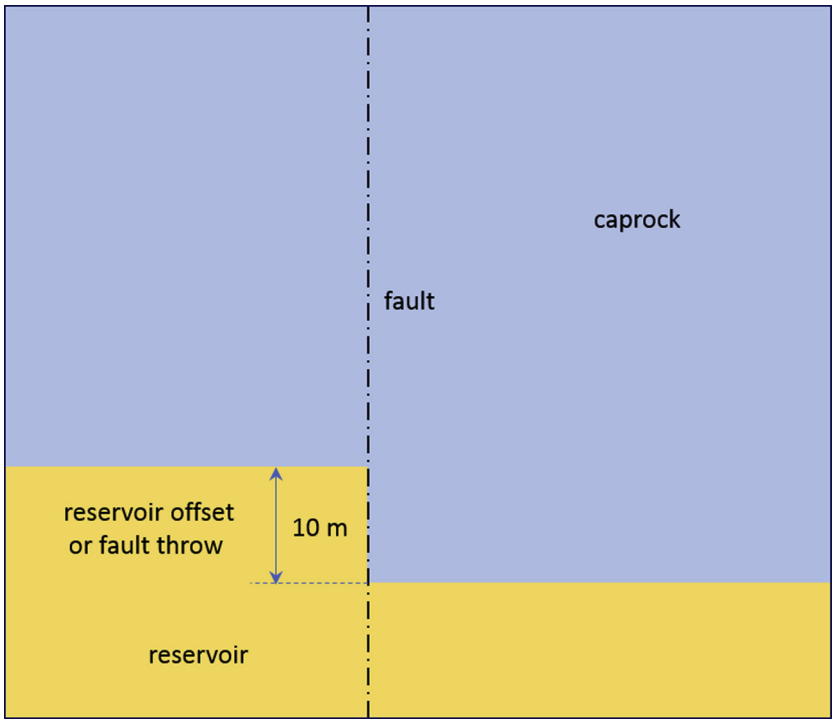

Fig. 4. Sketch of the geometry used for simulations around a reservoir offset of 10 m. The caprock (blue) is on top of the reservoir (orange). The black dashed line indicates a possible fault plane related to the reservoir offset. The area simulated is 50 m wide and 50 m high. We used a Dirichlet boundary condition at the reservoir-caprock interface for the flow. For the flow at the left and right boundary we used a zero flux boundary condition. For the poro-elastic equations we used a symmetry plane at the bottom, a zero horizontal displacement at the left and right boundaries and a free boundary at the top of the model.

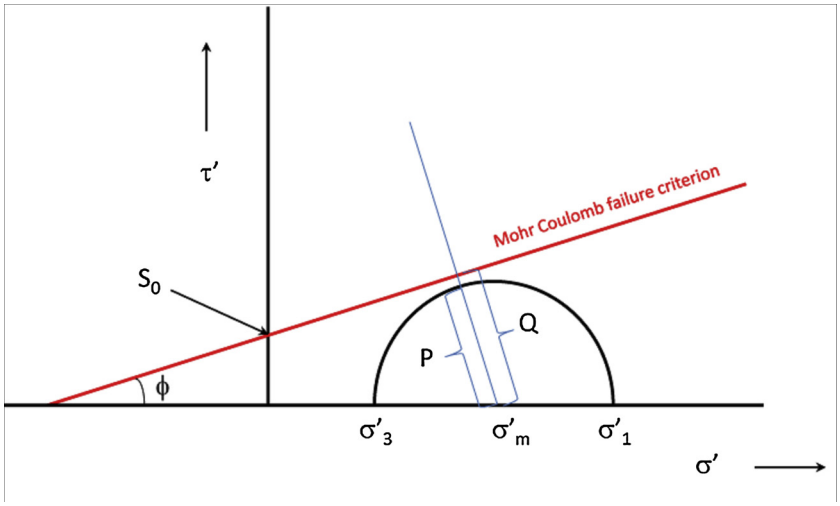

Fig. 5. Mohr diagram in the $\sigma' - \tau$ plane with the normal effective stress $\sigma' = \sigma - p_w$ along the horizontal axis and the shear stress τ along the vertical axis. The length of line P equals the radius of the Mohr circle $(\sigma'_1 - \sigma'_3)/2$ with the centre at $(\sigma'_1 + \sigma'_3)/2$. The length of line Q equals the shortest distance between the centre of the Mohr circle and the Mohr-Coulomb failure criterion line. The radius of the Mohr circle is equal to the shear stress $\tau = (\sigma'_1 - \sigma'_3)/2$. SCU can be calculated from the cohesion strength C_s and the friction angle φ. It equals the ratio between the lengths of two lines P and Q. SCU = 1 when the Mohr circle touches the Mohr-Coulomb failure line. Since σ'_1 and σ'_3 depend on the location in the caprock, SCU varies in the area around the reservoir offset.

3.3. Geometry

Fig. 4 shows the geometry of the reservoir-caprock interface with a moderate reservoir offset of 10 m which is considered typical for this field and below the seismic resolution. With emphasis on the physics of clay swelling, the diffusion process in the caprock at a similar reservoir offset was simulated by Wentinck and Busch (2017) using an axi-symmetric or cylindrical one-dimensional geometry. Using this simple one-dimensional geometry we obtained reasonable estimates for the stress build-up in the caprock around the offset following from CO_2 diffusion, keeping in mind that there are considerable uncertainties in other aspects of the model, such as the hydration state for the clay and the pressure recovery in the reservoir over time. In this work, we show the results of similar simulations but extended to two dimensions in convenient Cartesian coordinates by keeping in mind that the length of the offset along fault strike is much larger than the offset itself. As frequently done, the simulations are for a plane strain condition which means that there is zero strain along fault strike, i.e., in the direction perpendicular to the plane shown in Fig. 4.

The outer boundaries of the domain for the calculations also include the reservoir and are at a sufficient distance from the reservoir offset to have no significant effect on the stress-build up around the offset and on the CO_2 migration into the caprock. The reservoir and caprock are modelled as isotropic poro-elastic bodies with mechanical properties typical for the Captain sandstone and the Rodby mudrock, respectively.

3.4. Failure of the caprock

Swelling-induced stress changes may lead to shear failure of the caprock or to shear failure of pre-existing faults in the caprock. With no information about the strength of faults in the Rødby mudrock, we assume that these faults will fail under the same stress conditions as the relatively weak caprock and that their poro-elastic properties are the same as for the caprock. This means that the fault along the reservoir offset is not explicitly modelled as a plane of different weakness.

Assuming Mohr-Coulomb shear failure, the failure criterion for rock

is defined by the so-called shear capacity utilisation (SCU) (Busch et al., 2016), which is used in practice in Shell. Failure occurs when SCU > 1. This variable compares the actual level of shear stress τ with the shear stress capacity τ_{max} at a specific stress condition by the ratio (Fig. 5):

$$SCU = \frac{\tau}{\tau_{max}} = \frac{(\sigma'_1 - \sigma'_3)/2}{C_s \cos\phi + (\sigma'_1 + \sigma'_3)/2 \sin\phi} \quad (1)$$

$\sigma'_1 = \sigma_1 - p_w$ and $\sigma'_3 = \sigma_3 - p_w$ are maximum and minimum principal effective stresses in the caprock respectively. C_s and φ are the cohesion strength and friction angle of the caprock.

3.5. Field data and experimental data used in the simulations

The field stresses and hydrostatic pressure used in the simulations are typical for this field with the reservoir-caprock interface at about 2.5 km depth but not precise. In this part of the North Sea, the maximum and minimum horizontal field stresses are expected to be approximately the same and the main contribution to shear stress in the caprock results from a difference between the vertical and the horizontal field stresses (Rutqvist et al., 2016). Conservatively, the vertical and the minimum and maximum horizontal field stresses used are taken σ_v = 50 MPa and $\sigma_h = \sigma_H$ = 35 MPa, respectively. When the CO_2 plume reaches the reservoir-caprock interface, the pore pressure in the reservoir and caprock is taken p_w = 25 MPa, corresponding to a normal hydrostatic pressure. This leads to a ratio between the effective horizontal and effective vertical stresses of $(\sigma_v - p_w)/(\sigma_h - p_w) = 0.5$. This value is slightly lower than a value of 0.55, based on several studies for shales in the North Sea. The temperature in the reservoir and caprock is taken as 80 °C (Shell UK Ltd., 2014a).

Core analyses show that the Rødby mudrock contains 57 wt% smectite on average, see Table 1 but contains more carbonate rich layers with smectite contents less than 10 %. These are exceptionally high smectite contents (c.f. Fig. 1). To account for potentially lower smectite contents in the more silty layers in the caprock, we considered an average number of 30 wt%, demonstrating that the difference between 30 % and 57 % does not impact the outcome of this study.

The expressions for the chemical potentials of water and CO_2 in both pore volumes of the caprock, the transport properties of these species, the volumetric expansion of the interlayer space and the stress generated when this expansion is constrained are calibrated against experimental data, such as CO_2 sorption isotherms, heat of immersion experiments and CO_2 diffusion experiments, see Wentinck and Busch (2017). Volumetric expansion data have been obtained under hydrostatic reservoir conditions: 10–15% swelling is possible for an initial basal spacing d_{001} ~ 1.1 nm and about 4 % at d_{001} ~ 1.2 nm (Fig. 3). Swelling stress data have been obtained under nearly iso-volumetric (or zero-strain) reservoir conditions when the rock is exposed to CO_2. Of course, both experimental conditions are extreme stress conditions which differ from the real subsurface stress conditions in the caprock and from those in the simulations.

The volumetric expansion and generated stress depend very much on the intitial *in-situ* hydration state of the smectite. In particular, the substantial iso-volumetric swelling stresses of 35–80 MPa observed in laboratory-air moistured clay aggregates (Zhang et al., 2018) have not been observed for completely wet smectite. Since the *in-situ* hydration state of the smectite can only be approximated from thermodynamic considerations as explained by Bird (1984), this leaves us with a major uncertainty about the corresponding *in-situ* swelling stresses. According to thermodynamic considerations from Bird (1984), we expect for the hydration state of mono- and divalent smectites in the Rødby/U Valhall shales at about 2.5 km depth an initial basal spacing in the range 1–1.5 nm: we use an average value d_{001} = 1.2 nm.

The macropore porosity φ_w = 0.1 is typical for shaly caprocks. Conservatively, we take for the caprock an initial permeability $k_{w,0}$ = 50 nD which is 5 times a typical value for shaly caprocks (Busch and Amann-Hildenbrand (2013). Equally, the initial effective diffusion coefficient for CO_2 is taken $D_{w,0} = 5.0 \times 10^{-10}$ m^2/s which is also 5 times a typical value (Busch et al., 2008).

In general, k_w and D_w decrease with an increase in the mean effective stress $\Delta\sigma' = \sigma' - \sigma'_0$ and increase when there is shear failure. Herein, $\sigma' = (\sigma_1 + \sigma_2 + \sigma_3)/3 - p_w$ where $\sigma_1, \sigma_2, \sigma_3$ are the three principal stresses in the rock and p_w is the fluid pressure in the macropores. σ'_0 is the initial effective compressive stress. Our first attempt to include an increase of k_w and D_w by shear failure is by writing $k_w = k_{w,0} \cdot f(\Delta\sigma', SCU^+)$ and $D_w = D_{w,0} \cdot g(\Delta\sigma', SCU^+)$ where f and g are empirical functions of $\Delta\sigma'$ and SCU^+. Both variables are functions of space and time (**x**,t). The variable SCU^+(**x**,t') is the maximum value of SCU(**x**,t) in the time interval $0 \le t \le t'$. This means that we disregard healing processes in the caprock and that the effect of shear failure is irreversible. Lacking experimental data for changes in k_w and D_w of the Rødby mudrock under shear failure, we use in this study $f = g = f_1(\Delta\sigma') \cdot f_2(SCU^+)$ where

$$f_1(\Delta\sigma') = f_{1,min} + (1 - f_{1,min}) \exp(-C_k \Delta\sigma') \text{ and } f_2(SCU^+) = 1 + (f_{scu,max} - 1) f_t(SCU). \quad (2)$$

Herein f_t is a function of time. Within an insignificant time, f_t increases from zero to 1 when SCU exceeds the threshold value for shear type failure, i.e. SCU = 1. $f_{scu,max}$ is the maximum factor with which k_w and D_w can increase. For $\Delta\sigma' = 0$, $f_1(\Delta\sigma') = 1$. For $\Delta\sigma' \to \infty$, $f_1(\Delta\sigma') = f_{1,min}$ to ensure that values for k_w and D_w never drop below $f_{1,min}$.

For reference, we use in simulation A, $C_k = 0$ and $f_{scu,max} = 1$. So, in this simulation $\Delta\sigma'$ and SCU have no effect on k_w and D_w. In simulation B, we use $C_k = 0.2\,\text{MPa}^{-1}$ based on the following data: Values for clay rich shales from the illite-rich Wilcox formation from 4 km depth are in

Table 1
XRD analysis of selected caprock samples, including well names and sampling depth. Mineral abbreviations are in accordance with the abbreviations list published by Whitney and Evans (2010).

Well Name	Driller'sdepth (ft)	Descript.	Qz [m%]	Kfs [m%]	Ab [m%]	Ms + Ilt [m%]	Sme [m%]	Kln [m%]	Chl [m%]	Cal [m%]	Dol [m%]	Sd [m%]	Brt [m%]	Hl [m%]	Hem [m%]	CEC [meq/kg]
14/29a-4	8817	U Valhall - Captain contact	14	5.9	3.8	3.7	54.7	16	1.2	0	0	0	0	0.3	0.2	411
14/29a-4	8800.4	U Valhall Mbr	23.4	4.1	3	3.8	53.9	1.6	0.4	8.4	0.3	0	0.1	0.2	1	486
14/28b-2	8234.5	U Valhall Mbr	4.4	0	0	0	9	0	0	3	53.8	29.9	0	0	0	190
14/28b-2	8242	U Valhall Mbr	13.9	4.1	2.5	3.7	72.1	1	0.6	1.2	0.5	0	0.2	0.2	0.1	569
14/29a-4	8824.5	Captain E	11.6	3.6	2.9	3.3	59.6	6.9	0.7	8	0.1	0	0.1	0.2	2.9	533
14/29a-4	8815	U Valhall Mbr	18.4	3.8	2.6	2.1	53.5	2.1	2.5	13.2	0.1	0	0.2	0.2	1.3	467
14/29a-4	8809	U Valhall Mbr	21.2	4.5	4	2.9	51.9	1.7	1.9	11.2	0.2	0	0.2	0.1	0.3	384
14/29a-4	8772	Rødby	14.6	4.4	2.4	2.8	69.3	2.6	0.9	2.1	0.3	0	0.2	0.3	0.1	442
20/4b-6	8600-8610	U Valhall Mbr	16.8	4.6	2.3	4	49.3	6	2.5	11.7	0.6	0	0.6	1.2	0.2	411
14/29a-4	8813	U Valhall Mbr	22.6	3.8	3.1	2.8	60.5	0.3	1.3	4.6	0.4	0	0.3	0.2	0.3	556

the range $C_k = 0.05 - 0.5\,MPa^{-1}$ (Kwon et al., 2004); $C_k \sim 0.03\,MPa^{-1}$ for North Sea Whitby mudrocks due to the closure bedding parallel micro-crack like pores (McKernan et al., 2017); for Upper Jurasic Bossier shale with high clay content, $C_k = 0.01–0.06\,MPa^{-1}$ (Fink et al., 2017); for Devonian Marcellus and Ohio shales $C_k < 0.06\,MPa^{-1}$ (Chen et al., 2015). We use $f_{1,min} = 0.1$ to ensure that k_w and D_w never drop below 10 % of the initial values.

To include a possible significant increase of k_w and D_w under shear failure in simulation B, we use $f_{scu,max} = 20$.

The cohesion strength and friction angle for the caprock used are taken $C_s = 3\,MPa$ and $\varphi = 20°$. Typical values for the unconfined compressive strength of mudrock cores for several CCS projects are in the range 5–30 MPa but can be as low as 1 MPa and as high as 80 MPa. Friction angles are in the range 15–40° (Shell UK Ltd., 2014b). As mentioned earlier, we disregard the possibility that reactivated faults in the caprock are even weaker than this relatively weak rock. Young's modulus and Poisson ratio can vary broadly for weak and strong mudrocks and are in the range $E = 0.25–12\,GPa$ and $\nu = 0.14–0.4$, respectively (Bastiaens et al., 2006; Josh et al., 2012). These are typical values for mudrocks. We use $E = 5\,GPa$, $\nu = 0.35$ and a Biot constant $\alpha = 0.84$. For the sandstone reservoir rock, we use $E = 15\,GPa$, $\nu = 0.25$ and a Biot constant $\alpha = 0.72$.

3.6. Results of simulations

In this study we are only interested in CO_2 migration into the caprock and not in the migration of the CO_2 plume towards the reservoir-caprock interface by bouyancy forces. We expect that when the CO_2 plume reaches this interface around the reservoir offset, the CO_2 concentration at this interface builds up in time-scales on the order of several months to several years, which is relatively quick when compared to 10,000 years of CO_2 migration into the caprock. The final CO_2 concentration at the reservoir-caprock interface is in equilibrium with the hydrostatic reservoir pressure of the CO_2 plume. The fluid pressure p_w at the interface remains constant. Where the CO_2 concentration in the caprock is comparable with the final CO_2 concentration at the interface, the interlayer space of the clay expands and the effective stress increases. The expansion of the interlayer space coincides with an increase of the pressure in the interlayer space.

We show the results of two simulations A and B. As said, for the reference simulation A, k_w and D_w do not depend on $\Delta\sigma'$ and SCU^+. For simulation B, k_w and D_w do depend on $\Delta\sigma'$ and SCU^+. Figs. 6–8 show the main results. The figures show the adsorbed CO_2 concentration in the interlayer space of the clay (Fig. 6), the change in the effective stress (Fig. 7) and the shear capacity utilisation SCU in the caprock (Fig. 8). The figures are snapshots about 100, 1000 and 10,000 years after the CO_2 plume has reached the reservoir-caprock interface. Other variables, such as the volumetric strain, the pressures in the macropores and in the interlayer space, have values which are comparable with those presented in Wentinck and Busch (2017).

When there is no imposed pressure increase at the reservoir-caprock interface, CO_2 penetrates in the caprock from a few decimeters in 100 years to a few meters in 10,000 years, as shown in Fig. 6. This distance is significantly less than if there would be no adsorption of CO_2 in the clay. As shown in simulation B, the combined effect of effective stress and shear failure in the caprock due to the adsorption of CO_2 in the clay does not change the CO_2 penetration into the caprock dramatically with respect to simulation A. In both simulations, the penetration of CO_2 into the caprock is only over a small distance when compared to the thickness of the reservoir and the 117–165 m caprock (Rødby/U Valhall shales plus Hidra/Plenus marls).

Fig. 8 shows where shear failure around the reservoir offset can be expected based on shear capacity values SCU as defined by Eq. (1). The swelling stress either promotes or suppresses conditions for shear failure, in agreement with the results of axi-symmetric simulations shown in Wentinck and Busch (2017). In particular, swelling reduces the condition for shear failure along the horizontal parts of the reservoir-caprock interface, away from the offset, since the swelling stress primarily adds to the relatively low horizontal stress. On the other hand, swelling stress promotes failure just right from the reservoir offset because in this area the substantial compressive stress primarily adds to the higher vertical field stress and much less to the lower horizontal field stress.

During 10,000 years the area of possible shear failure slowly migrates from just right of the reservoir offset to the upper corner of the offset. This implies that the area $SCU^+ > 1$ is considerably larger than the area $SCU > 1$ in the snapshot at 10,000 years in Fig. 8. Above the upper corner of the offset $\Delta\sigma'$ does not increase much, as shown in Fig. 7, while the stress condition approaches shear failure. This leads to an increase of k_w and D_w and thus to a moderate additional progress of the diffusion front above the upper corner of the offset, as shown in Fig. 6 for simulation B.

As mentioned earlier, there is a major uncertainty about the *in-situ* hydration state of the smectities in the caprock and consequently about the maximum *in-situ* swelling stress generated. If the *in-situ* hydration state is between the saturation state of laboratory-air moistured clay and fully wetted clay, the substantial swelling stress calculated here cannot be ruled out and the results shown in these figures should be considered representative. It is well possible that the hydration state is higher. In this case, the generated stresses will be considerably lower. This is an area of research requiring future work. We take this as an uncertainty for the risk assessment and passive safeguarding procedure that might however be irrelevant for this specific case study considering other passive safeguards preventing shear failure within the caprock.

4. TESLA safeguarding assessment for the peterhead CCS storage seal

Methods for risk assessment can be quantitative or qualitative. To perform a robust quantitative risk assessment, historical performance data are required to provide empirical evidence for the occurrence frequency of rare events. In this study, the TESLA (Technical Evidence Support Logic Assessment) method (Tucker et al., 2013) is used which is a typical evidence and logic based industry workflow used in FEED studies, where the uncertainty is evaluated against (i) the evidence to support a hypothesis (typically indicated in green), (ii) the evidence to refute a hypothesis (typically indicated in red) and (iii) the remaining uncertainty (typically indicated in orange or colorless). The sum of the three criteria is 100 %. It is the task of the FEED study to reduce the remaining uncertainty and to develop methodologies and workflows to potentially actively manage the risk. A risk assessment then builds on such a technical assessment.

Based on the modelling effort described above a safeguarding procedure has been applied to manage the threat of CO_2-induced clay swelling. This threat has been identified to potentially cause a risk for CO_2 containment by causing shear failure in the case where specific conditions are met. These conditions are summarised below and discussed separately with respect to the Goldeneye storage complex of the Peterhead CCS project considered previously.

1 **The mineralogy of the caprock**. Smectite content within the primary caprock may be insufficient to cause enough swelling to create shear failure. The task is therefore to accurately determine the clay mineralogy and content. We recommend evaluating the geometry of the seal and pre-existing faults, and the mechanical and transport properties of the seal if the formation contains more than 20 wt% smectite. This is based on the large swelling stresses of tens of MPa that may develop in smectites (see Zhang et al., 2018). This criterion may be relaxed if swelling stress measurements on site-specific material (mudrock) indicate low strain and stress values due to the CO_2-clay interaction.
2 **The geometry and stress condition of the caprock**. Even with

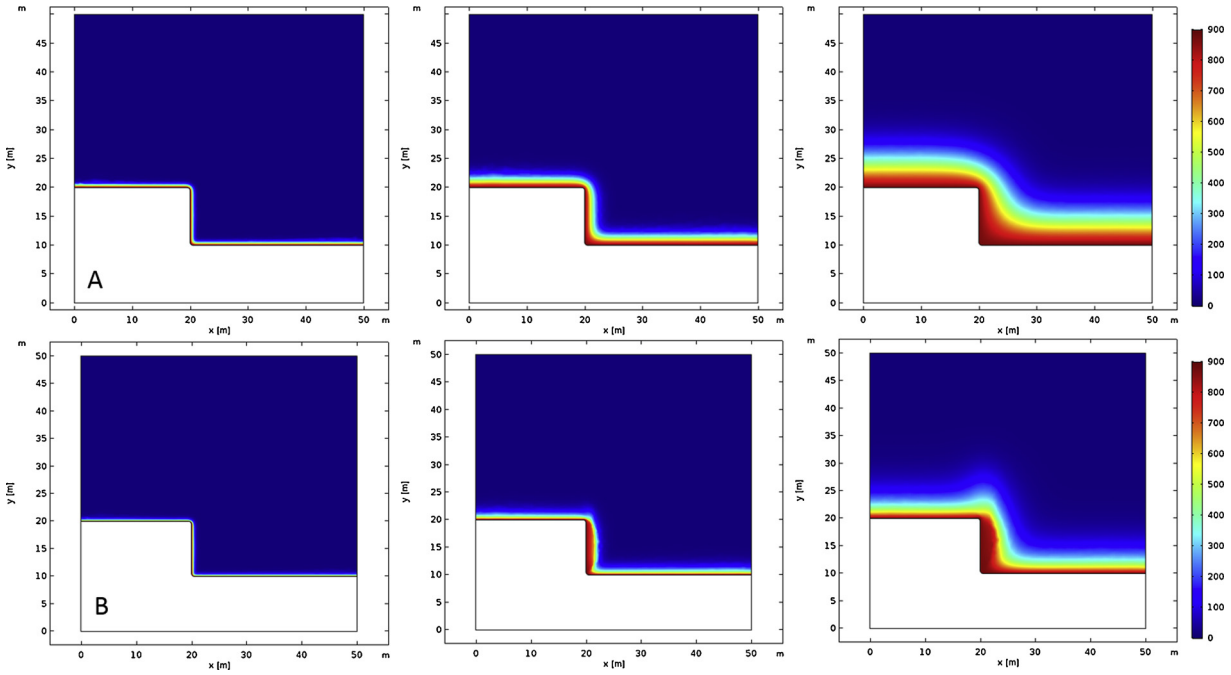

Fig. 6. Adsorbed CO_2 concentration in the caprock c'_{sB} [mol/m^3] after about 100, 1000 and 10,000 years according to simulations A and B. For simulation A, the permeability k_w and diffusion coefficient D_w are taken constant. For simulation B, k_w and D_w depend on $\Delta\sigma'$ and SCU^+ according to Eq. (2), meaning $C_k = 0.2\,MPa^{-1}$, $f_{1,min} = 0.1$ and $f_{scu,max} = 20$. For simulation A, CO_2 penetrates in 10,000 years over a distance of about 5 m in the caprock. For simulation B, CO_2 penetration is comparable albeit that farther away from the offset it is less because of an increase in the compressive effective stress. Above the upper corner of the offset, there is some additional progress of the diffusion front due to an increase of D_w in this area. The increase of D_w follows from an increase in SCU^+ while an increase in $\Delta\sigma'$ in this area is relatively small.

sufficient smectite in the storage seal, clay swelling only creates a build-up in shear stresses that extends across the entire thickness of the storage seal if there is a significant discontinuity in the storage seal, e.g. a fault, with an off ;set comparable to, but less than, the thickness of the storage seal itself. For these geometries we need to understand how swelling-induced stresses contribute to the existing field stress in the caprock. Seismic interpretations of the storage seal geometry should reveal the presence or absence of these geometries within the region of the CO_2 plume. Regional stress maps and borehole breakout or fracture data can be used to estimate the post-hydrocarbon production or present-day stress state in the caprock.

3 **The mechanical behaviour of the caprock**. If sufficient smectite is

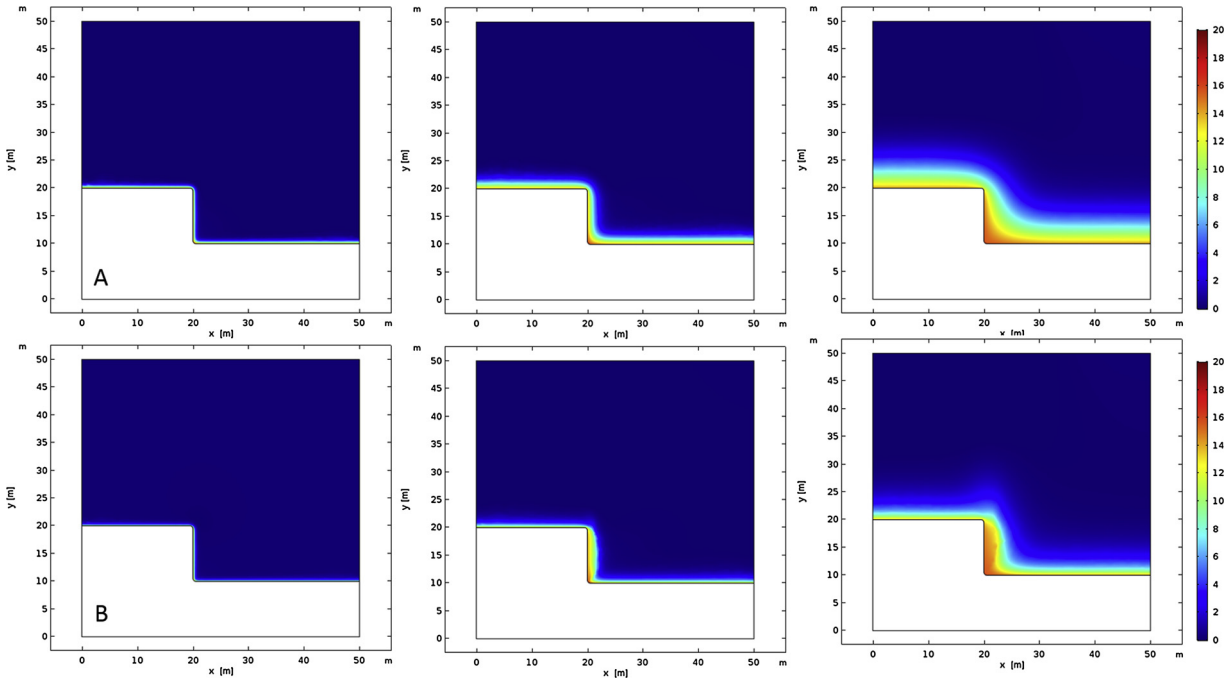

Fig. 7. Change in the effective stress $\Delta\sigma'$ [MPa] after about 100, 1000 and 10,000 years according to simulations A and B. For simulation A, the permeability k_w and diffusion coefficient D_w are taken as constant. For simulation B, k_w and D_w depend on $\Delta\sigma'$ and SCU^+ according to Eq. (2), meaning $C_k = 0.2\,MPa^{-1}$, $f_{1,min} = 0.1$ and $f_{scu,max} = 20$. Particularly, around the lower corner of the reservoir offset, the effective compressive stress $\Delta\sigma'$ builds up.

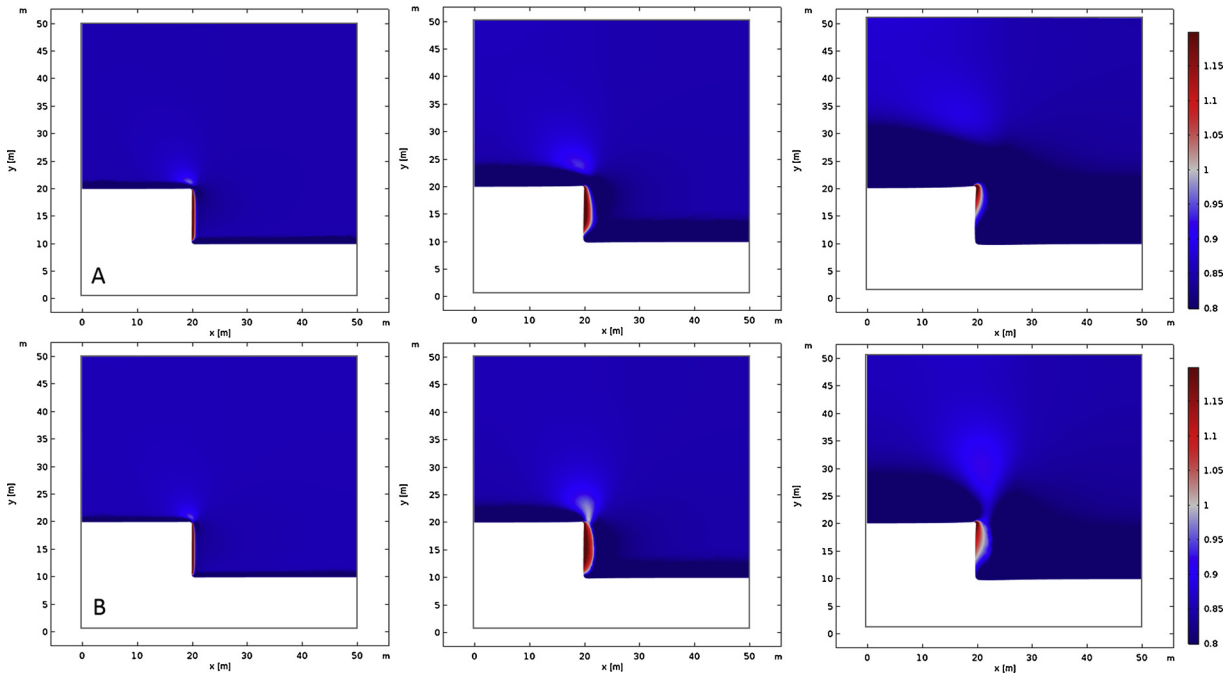

Fig. 8. Shear capacity utilisation SCU [-], as defined by Eq. (1) after about 100, 1000 and 10,000 years according to simulations A and B. For simulation A, the permeability k_w and diffusion coefficient D_w are taken constant. For simulation B, k_w and D_w depend on $\Delta\sigma'$ and SCU^+ according to Eq. (2), meaning $C_k = 0.2\,MPa^{-1}$, $f_{1,min} = 0.1$ and $f_{scu,max} = 20$.
The area where shear failure takes place migrates from just right from the reservoir offset to the upper corner of the offset.

present and a substantial offset geometry exists, creep deformation in the caprock may relax the induced shear stress, potentially reducing the risk of brittle shear failure within the storage seal. When the rate of shear stress development is controlled by diff ;usion, our simulations show that it would take about 100–10,000 years to affect a substantial rock volume. Note that the permeability, diffusion coefficient and smectite content in more ductile caprock can be significantly higher. Suitable laboratory experiments should reveal the long-term creep behaviour of the caprock material, preferably when exposed to CO_2.

4 **The permeability in the shear zone of the caprock**. If the criteria 1–3 are met and shear failure occurs, it may still not lead to a significant permeability increase and hence create a leakage pathway to the aquifer formation above the caprock. Suitable laboratory experiments should reveal permeability changes associated with (slow) shear failure of the seal material.

4.1. Caprock mineralogy

4.1.1. Evaluation task

Quantifying the smectite content of the basal unit of the seal overlying the storage site, i.e. the Upper Valhall and Rødby shales.

4.1.2. Results

The mineralogical composition has been determined at RWTH Aachen University, Institute of Clay and Interface Mineralogy. Mineral quantification was performed on diffraction patterns from random powder preparates. The mineral compositions and cation exchange capacities of the analysed samples are reported in Table 1. The clay content of the samples is dominated by smectite (49–72 wt%). The smectite does not show significant mixed-layering with illite or other non-expandable clays. Its basal, or 001 reflection, is at $14-15$ Å in air-dried, Mg-exchanged oriented mounts and expands to > 18 Å upon glycerol saturation. Higher order 00 l reflections constitute a rational series. The random powder measurements yielded 060 reflections at about 1.50–1.51 Å for all samples, which is characteristic of dioctahedral smectites. The high smectite content, which is rather uncommon for mudrocks at these depths, is confirmed by the CEC-measurements. Illite-muscovite is present in much lower contents in most samples. Minor amounts of kaolinite were observed in all samples. One sample (14-29a-4, 8817 ft), which is right at the contact with the Captain member, has an exceptionally high kaolinite content (16 wt%) compared to the rest of the set. Chlorite was detected in trace amounts in all samples.

The mineralogical composition of sample 14/28b-2, 8234.5 ft differs substantially from the rest of the sample set. This sample is from a concretion consisting mostly of dolomite and siderite with uncommon cell parameters. In summary, high smectite contents in the Upper Valhall and Rødby shales are confirmed and even higher than expected based on the preliminary measurements. It was shown that, besides one concretion, all samples have high smectite contents, averaging approximately 57 wt%.

4.2. Caprock geometry

4.2.1. Evaluation task

Seismic interpretation of the caprock geometry to determine the presence or absence of a large offset within the caprock within the region of the CO_2 plume.

4.2.2. Results

The Rødby Formation together with the underlying Upper Valhall Shale Member are treated as the caprock (primary seal) for the Captain Sandstone reservoir. Within the storage complex this forms the lower part of the storage seal whereas the upper part of the seal is comprised of mudstones and thin limestones of the Hidra Formation and marlstones of the Plenus Formation which extend across and beyond the reservoir area. Their thicknesses, as measured at different wells, are given in Table 2.

Shell U.K. Limited has performed an extensive seismic interpretation of the top Captain and the Hidra/Rødby horizons. It was concluded that where potential faults can be identified, fault displacement is up to

Table 2
Seal thicknesses (m) from the wells within the Goldeneye storage site and in the direct vicinity of the field.

Interval	Average	14/29A-2	14/29A-3	14/29A-4	20/4B-3	GYA01	GYA02	GYA03	GYA04	GYA05	14/29A-5	20/4B-6	20/4B-7
Rødby	56	41	59	34	62	51	56	72	55	52	53	73	68
Hidra/Plenus	108	102	89	104	127	108	98	122	103	97	109	102	133
Rødby /Upper Valhall	61	41	67	41	69	53	56	73	55	59	57	84	80
Total Seal	**169**	**143**	**156**	**146**	**197**	**161**	**154**	**195**	**157**	**156**	**166**	**186**	**212**

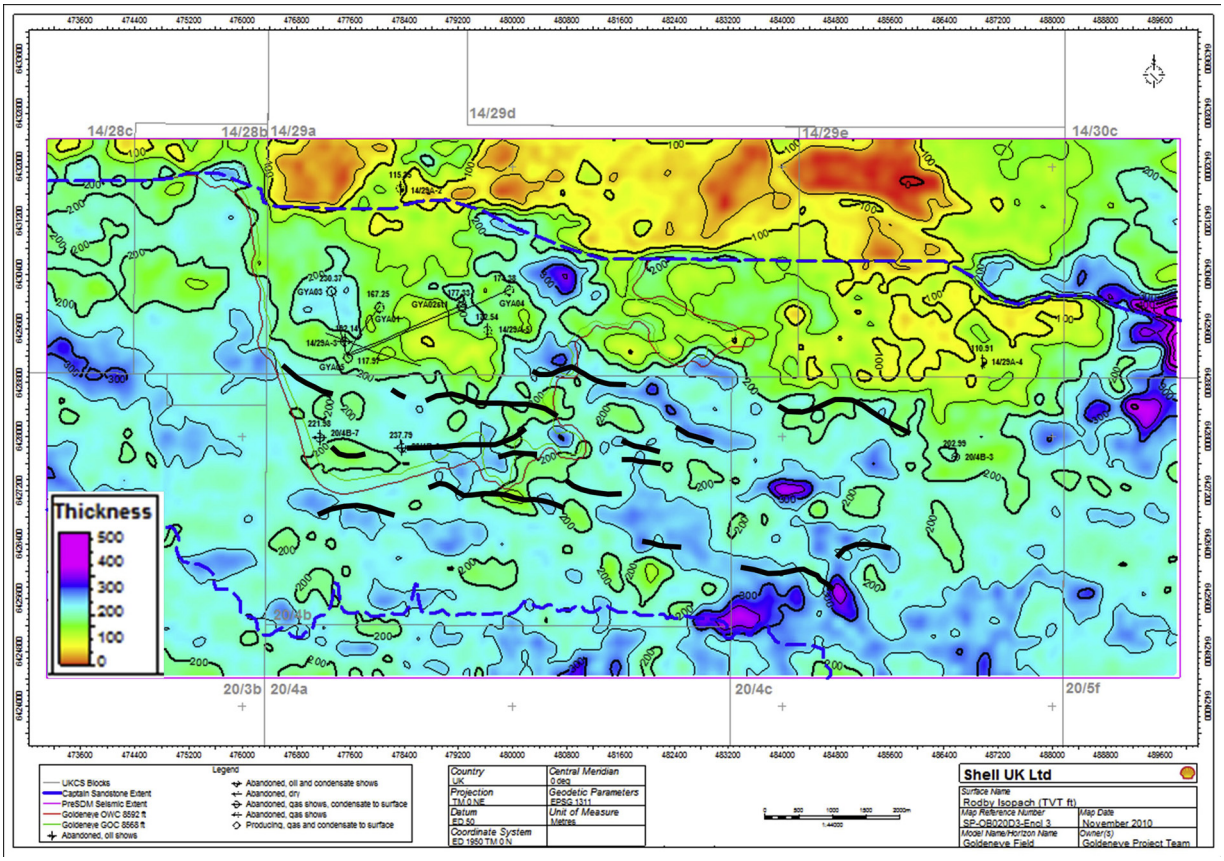

Fig. 9. Rødby Formation Isochore (lines of equal thickness) in feet, with top Rødby fault traces in black. Reservoir pinchout defined by blue dashed lines.

a maximum of one seismic loop (20 ms two-way-travel time), representing up to 33 m. The majority of faults have smaller displacements of 15 – 20 m. The Rødby caprock thickness in the vicinity of the mapped fault traces is shown in Figs. 9–11. The fault traces for the Captain D (the main storage interval) on Fig. 11 have been picked by a different interpreter in order to increase the range of possible faults captured.

Faults are only likely to provide an offset of the Rødby/Upper Valhall caprock when the caprock is thinner than 35 – 40 m (100 – 130 ft). This is because the seismic does not show fault offsets larger than this, while the seismic resolution does not allow the observation of smaller offsets. Only the most northerly fault in Fig. 11 qualifies and only in the case that the northern pinchout line for the Captain Formation (blue dashes) lies further north than currently mapped. Coupled with the significant thickness of overlying Lower Chalk (Hidra and Plenus Marls, average 169 m), which is also of sealing capacity, the likelihood of a fault having offset enough to completely offset the seal is remote.

4.3. Geomechanical behaviour: mudrock creep

4.3.1. Evaluation task

Compile suitable laboratory data about the likely creep behaviour of the caprock material.

4.3.2. Results

In principle it can be expected that the higher the smectite content the higher the swelling stress that would develop. At the same time, increased stress may lead to creep of the mudrock, allowing stress build-up to relax with time. If creep can compensate for stress build-up, which is diffusion-driven, the risk for shear failure, and the potential for associated leakage, can be considered low. Assuming that the CO_2 injection pressure in the Goldeneye would have remained below the minimum horizontal stress, and hence that fracturing of the intact caprock by pressurisation alone is unlikely, it is necessary to evaluate the extent to which swelling pressures can be dissipated via creep. A simple definition of creep is deformation at constant effective stress and it is difficult to predict the extent of creep needed to reduce ("relax") pressure build-up due to clay swelling. Unfortunately no suitable Rødby shale sample material is available to perform mechanical experiments. As such, analogue material is used to infer the potential mechanical behaviour of the Goldeneye caprock material (Rybacki et al., 2017; Sone and Zoback, 2013, 2014).

Mechanical tests have shown that the hydration state significantly affects the strength of the rock, with the rock becoming stronger due to drying (Gräsle and Plischke, 2010; Zhang et al., 2007). On the one

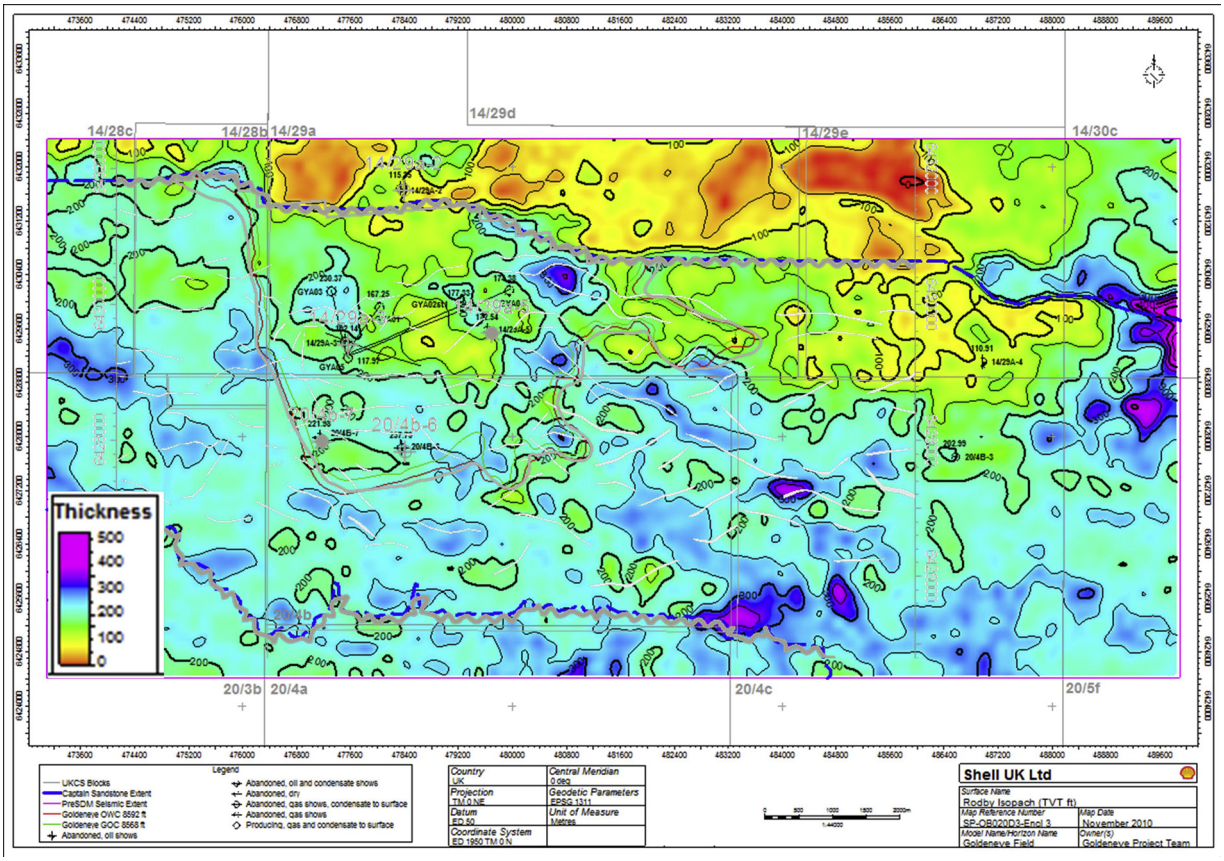

Fig. 10. Rødby Formation Isochores (lines of equal thickness) with top Captain fault traces in grey.

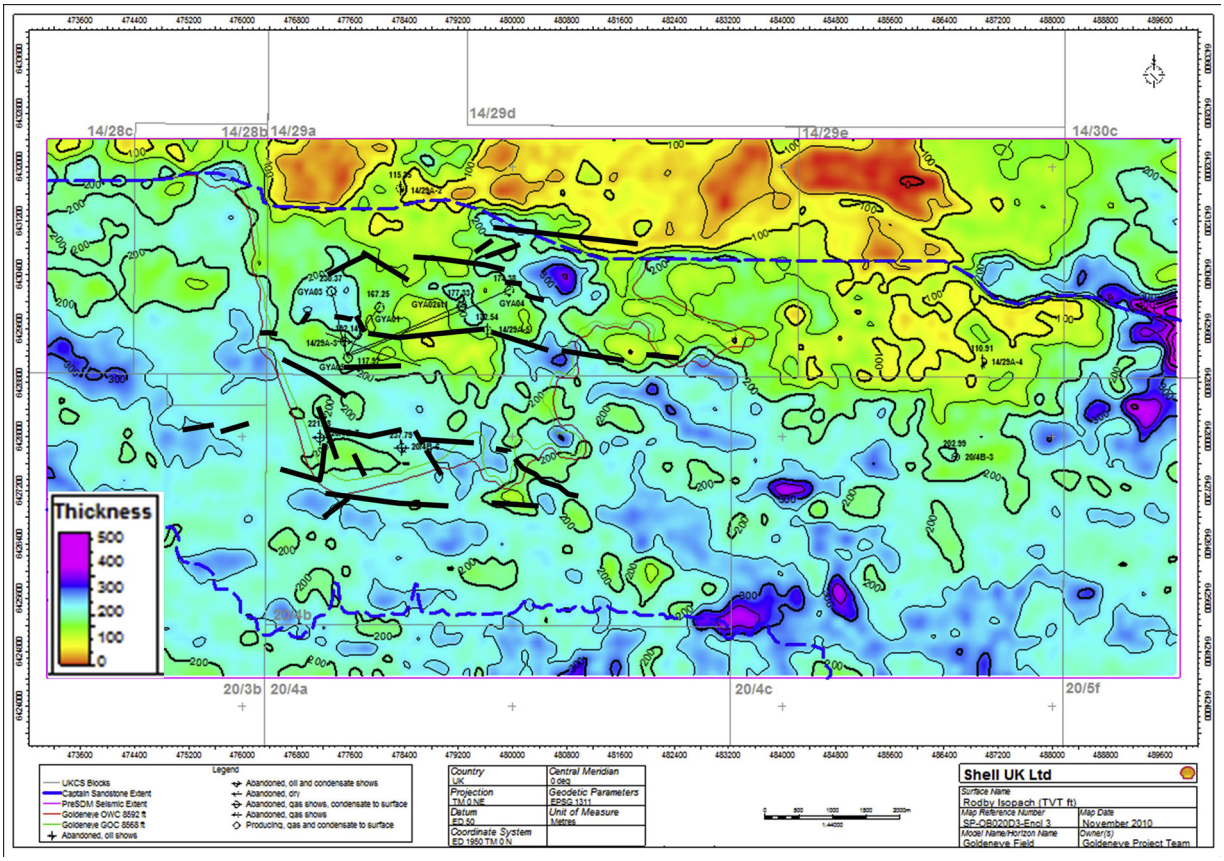

Fig. 11. Rødby Formation Isochores (lines of equal thickness) with top Captain D faults in black.

hand, drying appears to result in more creep and increased creep rate, as in the Opalinus Shale, probably due to collapse of the de-saturated pores (Zhang et al., 2007). By contrast, the presence of moisture is also observed to enhance time-dependent creep mechanisms, leading to higher strains and compaction rates as in in American gas shales (Sone and Zoback, 2014). This may have an impact on the creep behaviour of shale in the presence of CO_2, as carbon dioxide is able to take up small amounts of water (Wiebe and Gaddy, 1939), thereby potentially drying out the material. This however is rather realistic close to the injection well where dry CO_2 following injection of multiple pore volumes can dry out the formation. Further away from the injection well, CO_2 will likely be saturated with water, which prohibits further water uptake.

A potentially bigger role is reserved for the impact of mineralogical composition and temperature on rock strength and creep compliance, with higher clay content and temperature reducing rock strength but enhancing creep compliance. Creep appears to be accommodated by the deformation of weak minerals, such as clays, micas and organic matter (Rybacki et al., 2017; Sone and Zoback, 2014). Though the exact creep mechanism is not yet illucidated, it has been inferred that grain frictional sliding may play a role (Rybacki et al., 2017), made easier by the presence of frictionally-weak clay minerals (Rybacki et al., 2017; Tembe et al., 2010). The high clay content of the Rødby and Upper Valhall shales means they have a fairly low brittleness index (0.22, as determined using the empirical correlation from Rybacki et al. (2016)), indicative of a propensity for more ductile deformation (Rybacki et al., 2017). For high clay-content clays, such as the Haynesville and Barnett shales, predictions on stress relaxation in response to 0.1 % strain (i.e. comparable to the magnitude of induced swelling strain after 1 year of exposure, cf. Figs. 6 and 7), suggests that 20–60 % of the resulting stresses can be relaxed away within one day to a year. Given the high content of very frictionally-weak smectite (Moore and Lockner, 2007) in the Rødby and Upper Valhall shales, creep may be even more enhanced in these formations, meaning that relaxation occurs on shorter time scales. Furthermore, if faults are filled with fault gouge, creep may also be faster. To assess relaxation rates, it is necessary to obtain data on the compliance constant B and the power-law constant n (Sone and Zoback, 2014). In summary, although, in principle, ductile creep can compensate for the swelling-induced stress increase, reliable laboratory or field data at very low strain rates is lacking to assess its impact for stress- and strain-build-up in the caprock overlying the Goldeneye reservoir.

4.4. Fault permeability

4.4.1. Evaluation task

Compile laboratory data about the likely permeability changes associated with slow shear failure of the caprock material.

4.4.2. Results

Laboratory data on analogue material (Opalinus Shale) suggests that during shear failure, fracture permeability in this material may increase by orders of magnitude compared to the intact shale matrix permeability (Cuss et al., 2012). The permeability of the fault zone is strongly controlled by the relative proportions of fault core and damage zone (Caine et al., 1996), which for shale is more difficult to quantify than for more brittle low porosity rocks (Mitchell and Faulkner, 2012). However, recent coupled permeability-direct shear experiments on fault gouges (representative of the fault core) with a controlled composition show that the proportion of tectosilicate to phyllosilicate content impacts fault gouge permeability. As phyllosilicate content increases fault permeability decreases (Yi et al., 2018). Furthermore, with increasing sliding distance, gouge permeability decreases further (Bakker, 2017; Fang et al., 2017), both along and across the fault (Bakker, 2017). Even though composition poses a strong influence on frictional behaviour (Yi et al., 2018), geochemical modelling of the evolution of Opalinus Shale in response to CO_2-exposure suggests that fluid-rock interactions have only limited influence unless significant amounts of frictionally weak or unstable minerals are precipitated (Bakker et al., 2016, 2019). Fang et al. (2017) infer that for phyllosilicate-rich faults, weak particles, such as clays and micas, deform and get crushed into smaller particles, thereby filling the fault aperture. If these particles are then brought into contact with water or other swelling-inducing fluids, this may lead to fracture sealing.

The seal of the Goldeneye store contains minor amounts of quartz and carbonates (< 25 %) but high amiunts of clays, specifically frictionally weak, swelling smectite. These clays will likely lead to ductile failure and faults filled with weak minerals, resulting in a low fault core permeability. While the extent, geometry and permeability of a damage zone in shales has not been visualised and quantified yet, it is not unlikely that the ductile nature of the Rødby and Upper Valhall shales leads to a limited fracture network (Frash et al., 2016). In case a fault does become permeable, extends to shallower levels than the storage container, and the reservoir is at a pressure below the pressure in the seal, then dump flow into the reservoir will add to hydrostatic pressure recovery. As a consequence the reservoir will build up normal pressure much quicker. Such dump flow may change the pressure profiles over time but depends on fault permeability and the length at which the fault crosscuts the seal. In general, pressure recovery of the reservoir can occur on long or short time scales, depending on the hydrodynamic connectivity of the reservoir and fluid flow into the reservoir from overlying units along a permeable fault.

By contrast, it is possible that the gas column of injected CO_2 will create an additional pressure at the seal that exceeds the hydrostatic pressure in the seal after pressure recovery. This overpressure is determined by the density contrast between brine and CO_2 in the reservoir (Busch and Amann-Hildenbrand, 2013). For the Goldeneye reservoir, reservoir simulations predict a gas column height h on the order of $\sim$120 m (Shell UK Ltd., 2014a). Assuming a CO_2 density ρ_{CO2} of $\sim$700 kg/m^3 and a brine density ρ_{brine} of $\sim$1000 kg/m^3, we can calculate an excess pressure of $P_e = h(\rho_{brine} - \rho_{CO2})g = 0.35$ MPa, with g being the acceleration due to gravity. According to the Peterhead Storage Permit Application (Shell UK Ltd., 2014a), this additional pressure can, for one model scenario, lead to CO_2 pressures above initial hydrostatic reservoir pressure after 1000 years. As a result, if a fault becomes permeable, the driving force for viscous flow along the fault is possible, even if it occurs at slow rates and for small volumes.

For leakage out of the storage site to occur, all of the above four criteria need to be met. If leakage does occur through the base of the caprock (Rødby and Upper Valhall units) and reaches the upper part of the storage seal (Hidra and Plenus marls), little is known about the sealing integrity of these layers in the presence of CO_2. An analogue study for the Hidra and Plenus marls performed on Cretaceous marlstones from the Munster Basin in Germany (Wollenweber et al., 2010) indicated that when percolating CO_2 through plug samples, diffusion coefficients increase and capillary entry pressures decrease, indicating some minor integrity impairment. The results have not been verified by other studies, nor has a geochemical modelling study been performed for the Hidra and Plenus marls. Therefore reaction rates for the secondary seal remain uncertain. Given that the caprock contains significant amounts of smectite, it is likely that the secondary seal does as well. When in contact with CO_2, this may have a positive feedback on the fractures identified from BHI logs. While these fractures appear to be non-pervasive, i.e. they do not crosscut the formation, swelling may further limit the penetration of CO_2 into the formations.

5. TESLA risk assessment

The TESLA risk assessment is a process used to collect evidence for a hypothesis, and to quantify the evidence in support of or against this hypothesis, as well as the uncertainty in the evidence. It also aims at providing a quick and comprehensive overview of the level of information and evidence available and the likelihood of a risk. In this

Table 3
TESLA (Technical Evidence Support Logic Assessment) risk assessment matrix for CO_2-induced swelling of shale applied to the Goldeneye storage complex. The colour coding is not supposed to be the same as in Risk Assessment Matrices. In this table below, RED indicates that the threat remains, ORANGE indicates uncertainties remaining, and GREEN means that no risk is to be expected.

Passive safeguards[a]	Argument	Evidence for argument	Evidence against argument	Outcome	TESLA classification
Mineralogy	The quantity of smectite within the storage seal may be insufficient to cause enough swelling.	None	Detailed laboratory studies on caprock samples clearly confirm the presence of significant amount of smectite (57wt-%).	High smectite contents proven, significant swelling strain and stress likely. Uncertainties in subsurface hydration state.	
Geometry	If not compliant with the above, clay swelling only creates a build-up in shear stresses that extends across the entire thickness of the storage seal if there is a significant discontinuity in the storage seal, e.g. a fault, with an offset comparable to the thickness of the storage seal itself.	Faults with throws of up to 33 m have been mapped in parts of this structure: The mapped caprock (U. Valhall/Rødby, lower part of the seal) thickness is greater than the maximum throws of 33 m, except if the reservoir were to extend further than currently mapped in the NE. The integrity of the upper part of the seal (Hidra/Plenus) extending across the whole storage site is good, based on analogue fields, with a total thickness in excess of possible fault offsets.	The lower part of the seal (U. Valhall/Rødby Fms) is thin enough to be offset by mapped possible faults in a limited area at the extreme NE of their possible occurrence; shear failure for this part of the storage seal would therefore be possible. The integrity of the upper part of the seal (Hidra & Plenus) is considered good, but on the basis of analogue fields only.	Threat can be excluded for entire storage seal but a low possibility remains if Rødby/U Valhall shales were the only seal; note that on the basis of hydrocarbon analogue field data the sealing properties of the overlying Hidra & Plenus are considered to be good. Uncertainties are in the North of the reservoir, where the caprock thickness decreases.	
Plasticity	If not compliant with the above, plastic deformation mechanisms in the caprock may relax the induced shear stress to prevent brittle shear type failure within the storage seal.	The higher the smectite content the softer the shale; it is therefore more likely that swelling stress generated can relax into the shale matrix, i.e. more plastic creep.	Analogue data to the Rødby/U Valhall shales are rare/lacking from literature; no direct assessment possible at this point.	This remains a topic of high uncertainty and no consistent or suitable analogue data identified. We recommend performing detailed literature and lab studies.	
Permeability	If not compliant with the above, shear type failure may not develop fault permeability.	A sufficiently large area of a fault needs to undergo shear failure in order to develop permeability along fault; even if permeability would develop, flux rates could be below the detection limits of the monitoring installations.	CO_2 in the reservoir results in a gas column that will always exert a small overpressure (<0.5 MPa) to the caprock following hydrostatic pressure recovery. Therefore, if the fault is permeable it will leak with small but significant flux rates, based on analogue and conceptual data.	This remains a topic of high uncertainty and an R&D effort is needed to solve this issue	
Summary	If not compliant with all of the above, clay swelling will not build up a swelling pressure that is significant enough to cause shear failure of the seal. Further reservoir geometry will not allow fault reactivation and there is no permeability or pressure drive to cause CO_2 to leak.	The geometry of the reservoir (seal thickness versus potential fault offset) does not allow shear failure for the entire seal sequence to occur. Only in the very North of the reservoir a small likelyhood remains that fault offset is comparable to the thickness of the lower part of the seal (U. Valhall/Rødby Fms).	Smectite content could be sufficient to obtain shear failure and if the fault would become permeable, the possibility for a pressure-drive for fault leakage cannot be excluded.	Clay swelling following shear failure and the development of a permeable fault remains uncertain due to many parameters that cannot be quantified. For the Goldeneye reservoir, however, it is found that potential faults are below the thickness of the entire seal and a low risk remains only for the caprock. Loss of containment can therefore be classified as a low geological risk	

[a]Passive Safeguards are "natural" or geological criteria to lower a certain risk for a specific project, i.e. a risk is lowered or eliminated when, for instance in our case, no swelling clays would be present in the caprock that could cause shear failure and leakage.

case the risk is shear failure of faults activated by clay swelling, potentially leading to transmissive leak paths across the caprock of the Goldeneye storage complext. This assessment is summarised in Table 3 and is based on the discussions stated in Section 4.

6. Recommendations for future work

The following points deserve consideration for further studies to strengthen the confidence in seal integrity for smectite-rich shales. We consider the likelihood of fault reactivation by slip on pre-existing fault fractures and the creation of a permeable fault for the Goldeneye caprock to be low under the injection plans considered. However, a change in injection strategy towards higher volumes, or similar projects in similar formations in the North Sea, might raise similar concerns. Addressing the points below will support assessment of the clay swelling threat and the associated potential risk of loss of containment.

- As has been done for the Peterhead CCS project, it is highly recommended to obtain good and reliable mineralogy data for the seal (and also reservoir) formations. Not all commercial labs might be equipped and skilled to determine the clay mineralogy to the standard that is needed for obtaining reliable/accurate smectite compositions. In addition, reactive transport modelling relies on mineralogical input. The more reliable this input the more reliable any reactive transport modelling efforts.
- One major uncertainty of the clay swelling risk is the hydration state of swelling clays in the subsurface and under the vertical stress conditions present. We found that swelling strain (and potentially stress) is largest where the hydration state of clays is in-between discrete hydration states, i.e. where ~100 % of the clay interlayers are either occupied with zero, one or two water layers (Busch et al., 2016). Rough estimations of the hydration states for different burial depth and interlayer cations exist (Bird, 1984; Wentinck and Busch, 2017), however they only provide an approximation.
- Geomechanical parameters and data on shale is limited in the open literature. This is especially true for shale samples composed of high smectite content, like for the Rødby/Upper Valhall mudrocks. Adequate mechanical laboratory testing relies on sufficient sample

material (in the form of plugs), which is not available from cores drilled into or close to the Goldeneye reservoir. Although some caprock core was obtained, the material has degraded due to several years of exposure to atmospheric conditions, causing sample dehydration, and the preparation of suitable plugs is impossible. Currently, it will be extremely difficult to obtain *representative* core material to determine rock strength or creep parameters for predicting swelling stress relaxation into the shale matrix.

- Little information is available on the permeability along-fault which is induced by clay-swelling. We note that this permeability will essentially be zero if there is no driving force, i.e. a reservoir pressure exceeding the pressure in the fault or in higher formations. If however any future strategy includes pressurisation of the reservoir above hydrostatic, upward flow can occur along the shear fault gouge if there is sufficient along-fault permeability. A concise literature and modelling study might help reducing some of the uncertainties and would also help reducing this uncertainty.
- Insufficient information is available on the mineralogy, permeability, reactivity, or mechanical behaviour of the Hidra and Plenus marls overlying the caprock and forming the secondary seal. It was shown, and discussed above, that these formations act as seals for hydrocarbons for geological time scales but their reactivity with CO_2 is not investigated systematically and therefore not well understood. If good quality core sample material is available, corresponding laboratory tests could be conducted and reactive transport modeling scenarios be performed. This would support an improved understanding of the potential case when shear failure will occur in the shale caprock and CO_2 leaking across these formations, forming part of the storage seal.
- In the case that a permeable fault is not leaking fluids to overlying formations, due to insufficient pressure drive, it could support the re-pressurisation of the reservoir by so called dump flow, which is flow from higher to lower formations, due to an inward pressure gradient. Depending on fault permeability and areal extend such dump flow can be high over 100's to 1000's of years and might support reservoir pressure builup, potentially even to hydrostatic pressure. Specific case studies should be included in reservoir modelling to map conditions under which this is of relevance.

7. Conclusions

We applied the passive safeguarding procedure for clay swelling and potential shear failure in the caprock associated with possible fault offset (fault reactivation) to the Goldeneye storage complex. This complex was considered by Shell UK for storing approximately 1 millions tons of CO_2 annually, for a period of 10 years. The procedure gives reasonable confidence that in the context of injection plans considered, fault reactivation would be unlikely. We also identified uncertainties that need further investigation in future studies:

1 High-quality analyses of the caprock (Upper Valhall Shale and Rødby Formation) show a significant swelling clay content ($\sim$57 wt %). This can pose the risk of fault reactivation due to clay swelling in contact with CO_2 but only if there are faults in the caprock capable of offsetting a similar distance than the seal thickness; if creep of the fractured caprock cannot absorb the swelling strain and relax the building stresses; and if there is sufficient fault permeability coupled with a pressure differential to allow flow out of the reservoir.
2 Three rounds of fault interpretation covering the Rødby and the Captain Formations show that only one identified fault occurs in an area where the lower primary seal (Rødby/Upper Valhall) is of a thickness close to the maximum likely fault offset and that is in an area where the reservoir may not actually be present. In such a case, the upper part of the primary seal (Hidra & Plenus Marl) provides ample additional thickness to prevent full seal offset.
3 While the mineralogy and therefore swelling clay content is straightforward to determine, creep behaviour of the storage seal is not, and analogue data seems to be insufficient for direct correlation.
4 Following pressure recovery after reservoir abandonment, the gas pressure at the reservoir/seal interface may be higher than the hydrostatic pressure, providing the pressure drive for potential viscous flow along any potentially permeable fault. The controls on fault permeability in the presence of CO_2 are not well understood: clays in general are good fault seals and there is a fair chance that the high smectite contents of the Upper Valhall and the Rødby are beneficial for self-sealing, preventing upward flow along the fault gouge.

Declaration of Competing Interest

None.

Acknowledgements

We thank Shell Global Solutions for the permission to publish this work. O. Tucker and M. Dean provided valuable comments on an earlier version of this manuscript. This study has been partly subsidized through the ERANET Cofund ACT (Project no. 271497). Support is greatly acknowledged.

References

Altaner, S.P., Ylagan, R.F., 1997. Comparison of structural models of mixed-layer illite/smectite and reaction mechanisms of smectite illitization. Clays Clay Miner. 45, 517–533.
Bakker, E., 2017. Frictional and Transport Properties of Simulated Faults in CO_2 Storage Reservoirs and Clay-Rich Caprocks. Dept. of Earth Sciences. Utrecht University, pp. 267.
Bakker, E., Hangx, S.J.T., Niemeijer, A.R., Spiers, C.J., 2016. Frictional behaviour and transport properties of simulated fault gouges derived from a natural CO2 reservoir. Int. J. Greenh. Gas Control. 54 (Part 1), 70–83.
Bakker, E., Kaszuba, J., den Hartog, S., Hangx, S., 2019. Chemo-mechanical behavior of clay-rich fault gouges affected by CO2-brine-rock interactions. Greenh. Gases Sci. Technol. 9, 19–36.
Bastiaens, W., Bernier, F., Li, X.L., 2006. An Overview of Long-Term HM Measurements Around HADES URF, EUROCK 2006 Multiphysics Coupling and Long Term Behaviour in Rock Mechanics. pp. 15–26.
Biot, M.A., 1962. Mechanics of deformation and acoustic propagation in porous media. J. Appl. Phys. 33, 1482–1498.
Bird, P., 1984. Hydration-phase diagrams and friction of montmorillonite under laboratory and geologic conditions, with implications for shale compaction, slope stability, and strength of fault gouge. Tectonophysics 107, 235–260.
Bird, R.B., Stewart, W.E., Lightfoot, E.N., 2007. Transport Phenomena. J. Wiley, New York.
Busch, A., Alles, S., Gensterblum, Y., Prinz, D., Dewhurst, D.N., Raven, M.D., Stanjek, H., Krooss, B.M., 2008. Carbon dioxide storage potential of shales. Int. J. Greenh. Gas Control. 2, 297–308.
Busch, A., Amann-Hildenbrand, A., 2013. Predicting capillarity of mudrocks. Mar. Pet. Geol. 45, 208–223.
Busch, A., Bertier, P., Gensterblum, Y., Rother, G., Spiers, C.J., Zhang, M., Wentinck, H.M., 2016. On sorption and swelling of CO2 in clays. Geomech. Geophys. Geo-Energy Geo-Resour. 2, 111–130.
Busch, A., Kampman, N., 2018. Migration and leakage of CO2 from deep geological storage sites. In: Vialle, S., Ajo-Franklin, J., Carey, J.W. (Eds.), Geological Carbon Storage.
Caine, J.S., Evans, J.P., Forster, C.B., 1996. Fault zone architecture and permeability structure. Geology 24, 1025–1028.
Casabianca, D., Cosgrove, J., 2012. A new method for top seals predictions in high-pressure hydrocarbon plays. Petrol. Geosci. 18, 43–57.
Chen, D., Pan, Z., Ye, Z., 2015. Dependence of gas shale fracture permeability on effective stress and reservoir pressure: model match and insights. Fuel 139, 383–392.
Commission of the European Communities, 2009. Directive of the European Parliament and of the Council on the Geological Storage of Carbon Dioxide and Amending. Council Directives 85/337/EEC, 96/61/EC, Directives 2000/60/EC, 2001/80/EC, 2004/35/EC, 2006/12/EC and Regulation (EC) No 1013/2006.
Cuss, R.J., Milodowski, A., Harrington, J.F., 2012. Fracture transmissivity as a function of normal and shear stress: first results in Opalinus clay. Phys. Chem. Earth Parts A/B/C 36, 1960–1971.
de Jong, S.M., Spiers, C.J., Busch, A., 2014. Development of swelling strain in smectite clays through exposure to carbon dioxide. Int. J. Greenh. Gas Control. 24, 149–161.
Fang, Y., Elsworth, D., Wang, C., Ishibashi, T., Fitts, J.P., 2017. Frictional stability-permeability relationships for fractures in shales. J. Geophys. Res.: Solid Earth 122,

1760–1776.
Fink, R., Krooss, B.M., Amann-Hildenbrand, A., 2017. Stress-Dependence of Porosity and Permeability of the Upper Jurassic Bossier Shale: an Experimental Study. Geological Society, London Special Publications 454.
Frash, L.P., Carey, J.W., Lei, Z., Rougier, E., Ickes, T., Viswanathan, H.S., 2016. High-stress triaxial direct-shear fracturing of Utica shale and in situ X-ray micro-tomography with permeability measurement. J. Geophys. Res. 121, 5493–5508.
Giesting, P., Guggenheim, S., Koster van Groos, A.F., Busch, A., 2012a. Interaction of carbon dioxide with Na-exchanged montmorillonite at pressures to 640 bars: Implications for CO2 sequestration. Int. J. Greenh. Gas Control. 8, 73–81.
Giesting, P., Guggenheim, S., Koster van Groos, A.F., Busch, A., 2012b. X-ray diffraction study of K- and Ca-exchanged montmorillonites in CO2 atmospheres. Environ. Sci. Technol. 46, 5623–5630.
Gräsle, W., Plischke, I., 2010. Laboratory Testing (LT) Experiment: Mechanical Behavior of Opalinus Clay, Final Report From Phases 6-14. NAGRA, pp. 89.
Josh, M., Esteban, L., Delle Piane, C., Sarout, J., Dewhurst, D.N., Clennell, M.B., 2012. Laboratory characterisation of shale properties. J. Pet. Sci. Eng. 88–89, 107–124.
Kampman, N., Busch, A., Bertier, P., Snippe, J., Hangx, S., Pipich, V., Di, Z., Rother, G., Harrington, J.F., Evans, J.P., Maskell, A., Chapman, H.J., Bickle, M.J., 2016. Observational evidence confirms modelling of the long-term integrity of CO2-reservoir caprocks. Nat. Commun. 7.
Kwon, O., Kronenberg, A.K., Gangi, A.F., Johnson, B., Herbert, B.E., 2004. Permeability of illite-bearing shale: 1. Anisotropy and effects of clay content and loading. J. Geophys. Res. 109 B10205-B10205.10219.
Laurich, B., Urai, J.L., Desbois, G., Vollmer, C., Nussbaum, C., 2014. Microstructural evolution of an incipient fault zone in Opalinus Clay: Insights from an optical and electron microscopic study of ion-beam polished samples from the main fault in the Mt-Terri underground research laboratory. J. Struct. Geol. 67 (Part A), 107–128.
Makhnenko, R.Y., Vilarrasa, V., Mylnikov, D., Laloui, L., 2017. Hydromechanical aspects of CO_2 breakthrough into clay-rich caprock. Energy Procedia 114, 3219–3228.
McKernan, R., Mecklenburgh, J., Rutter, E., Taylor, K., 2017. Microstructural Controls on the Pressure-Dependent Permeability of Whitby Mudstone. Geological Society, London Special Publications 454, SP454.415.
Mitchell, T.M., Faulkner, D.R., 2012. Towards quantifying the matrix permeability of fault damage zones in low porosity rocks. Earth Planet. Sci. Lett. 339–340, 24–31.
Moore, D.E., Lockner, D.A., 2007. Friction of the smectite clay montmorillonite. In: Dixon, T., Moore, C. (Eds.), The Seismogenic Zone of Subduction Thrust Faults. Columbia University Press, New York, pp. 317–345.
Pearson, M.J., 1990. Clay mineral distribution and provenance in Mesozoic and Tertiary mudrocks of the Moray Firth and northern North Sea. Clay Miner. 25, 519–541.
Pearson, M.J., Small, J.S., 1988. Illite-smectite diagenesis and palaeotemperatures in Northern North Sea Quaternary to mesozoic shale sequences. Clay Miner. 23, 109–132.
Pinnock, S.J., Clitheroe, A.R.J., Rose, P.T.S., 2003. The Captain Field, Block 13/22a, UK North Sea, United Kingdom Oil and Gas Fields, Commemorative Millennium Volume. Geological Society, London, pp. 431–441.
Rother, G., Ilton, E.S., Wallacher, D., Hauss, T., Schaef, H.T., Qafoku, O., Rosso, K.M., Felmy, A.R., Krukowski, E.G., Stack, A.G., Grimm, N., Bodnar, R.J., 2013. CO2 sorption to subsingle hydration layer montmorillonite clay studied by excess sorption and neutron diffraction measurements. Environ. Sci. Technol. 47, 205–211.
Rutqvist, J., Rinaldi, A.P., Cappa, F., Jeanne, P., Mazzoldi, A., Urpi, L., Guglielmi, Y., Vilarrasa, V., 2016. Fault activation and induced seismicity in geological carbon storage – lessons learned from recent modeling studies. J. Rock Mech. Geotech. Eng. 8, 789–804.
Rybacki, E., Herrmann, J., Wirth, R., Dresen, G., 2017. Creep of Posidonia shale at elevated pressure and temperature. Rock Mech. Rock Eng. 50, 3121–3140.
Rybacki, E., Meier, T., Dresen, G., 2016. What controls the mechanical properties of shale rocks? – part II: brittleness. J. Pet. Sci. Eng. 144, 39–58.
Schaef, H.T., Ilton, E.S., Qafoku, O., Martin, P.F., Felmy, A.R., Rosso, K.M., 2012. In situ XRD study of Ca2+ saturated montmorillonite (STX-1) exposed to anhydrous and wet supercritical carbon dioxide. Int. J. Greenh. Gas Control. 6, 220–229.
Shell UK Ltd, 2014a. Peterhead CCS Project-Storage Permit Application. https://www.gov.uk/government/publications/carbon-capture-and-storage-knowledge-sharing-technical-subsurface-and-well-engineering.
Shell UK Ltd, 2014b. Peterhead CCS Project: Geomechanics Report. . https://assets.publishing.service.gov.uk/government/uploads/system/uploads/attachment_data/file/531054/Peterhead_11.115_-_Geomechanics_Report.pdf.
Sone, H., Zoback, M.D., 2013. Mechanical properties of shale-gas reservoir rocks—part 2: ductile creep, brittle strength, and their relation to the elastic modulus. Geophysics 78, D393–D402.
Sone, H., Zoback, M.D., 2014. Time-dependent deformation of shale gas reservoir rocks and its long-term effect on the in situ state of stress. Int. J. Rock Mech. Min. Sci. 69, 120–132.
Tembe, S., Lockner, D.A., Wong, T.-F., 2010. Effect of clay content and mineralogy on frictional sliding behavior of simulated gouges: binary and ternary mixtures of quartz, illite, and montmorillonite. J. Geophys. Res. 115 B03416.
Tucker, O., Holley, M., Metcalfe, R., Hurst, S., 2013. Containment risk management for CO2 storage in a depleted gas field, UK North Sea. Energy Procedia 37, 4804–4817.
van Oort, E., 2003. On the physical and chemical stability of shales. J. Pet. Sci. Eng. 38, 213–235.
Wentinck, H.M., Busch, A., 2017. Modelling of CO2 Diffusion and Related Poro-Elastic Effects in a Smectite-Rich Cap Rock Above a Reservoir Used for CO2 Storage. Geological Society, London, pp. 155–173 Special Publications 454.
Whitney, D.L., Evans, B.W., 2010. Abbreviations for names of rock-forming minerals. Am. Mineral. 95, 185–187.
Wiebe, R., Gaddy, V.L., 1939. The solubility in water of carbon dioxide at 50, 75 and 100 °C, at pressures to 700 atmospheres. J. Am. Chem. Soc. 61, 315–318.
Wollenweber, J., Alles, S., Busch, A., Krooss, B.M., Stanjek, H., Littke, R., 2010. Experimental investigation of the CO2 sealing efficiency of caprocks. Int. J. Greenh. Gas Control. 4, 231–241.
Yi, F., Derek, E., Chaoyi, W., Yunzhong, J., 2018. Mineralogical controls on frictional strength, stability, and shear permeability evolution of fractures. J. Geophys. Res. 123, 3549–3563.
Zhang, C.-L., Rothfuchs, T., Jockwer, N., Wieczorek, K., Dittrich, J., Müller, J., Hartwig, L., Komischke, M., 2007. HE-D Experiment: Thermal Effects on the Opalinus Clay - A Joint Heating Experiment of ANDRA and GRS at the Mont Terri URL. NAGRA, pp. 206.
Zhang, M., de Jong, S.M., Spiers, C.J., Busch, A., Wentinck, H.M., 2018. Swelling stress development in confined smectite clays through exposure to CO2. Int. J. Greenh. Gas Control. 74, 49–61.